archive ouverte UNIGE
http://archive-ouverte.unige.ch

Article

Illite-smectite rich clay parageneses from Quaternary tunnel valley sediments of the Dutch Southern North Sea – mineral origin and paleoenvironment implications

SEGVIC, Branimir, BENVENUTI, Antonio, MOSCARIELLO, Andrea

Abstract

The Pleistocene sediment infill of elongated glacial incisions of the Southern North Sea (SNS) often is referred to as tunnel valleys (TV). Its depositional environment is not yet fully understood and present study addresses this challenge from a perspective of clay mineral transformation (illite to I-S) reported from the largest Elsterian TV of SNS. Material acquired from the K14-12 borehole in the Dutch offshore was analyzed by X-ray diffraction, electron microscopy, electron microprobe analyses, and laser particle-size analysis. Illite and illite-smectite appeared as dominant clays along with minor amounts of kaolinite, kaolinite-smectite, and chlorite. Highest amount of I-S is recognized in TV main portion, while in pre-glacial and uppermost deposits I-S is less abundant. The XRD peak fitting and deconvolution suggest I-S consists of several intermediates – ordered (well-crystallized illite + R3 I-S) and disordered (R0 I-S + R0 I-SS). Given the average particle sizes (> 2 μm) and Kübler index values (0.415-0.341°Δ2θ), illite as well as chlorite and kaolinite were interpreted as detrital. On the basis of I-S [...]

Reference

SEGVIC, Branimir, BENVENUTI, Antonio, MOSCARIELLO, Andrea. Illite-smectite rich clay parageneses from Quaternary tunnel valley sediments of the Dutch Southern North Sea – mineral origin and paleoenvironment implications. *Clays and clay minerals*, 2016

DOI : 10.1346/CCMN.2016.064026

Available at:
http://archive-ouverte.unige.ch/unige:88288

Disclaimer: layout of this document may differ from the published version.

UNIVERSITÉ DE GENÈVE

Manuscript
Click here to download Manuscript
MS_CCM_1032_Revised_Version_Clean.docx

Illite-smectite rich clay parageneses from Quaternary tunnel valley sediments of the Dutch Southern North Sea – mineral origin and paleoenvironment implications

Branimir ŠEGVIĆ, Antonio BENVENUTI, Andrea MOSCARIELLO

Department of Earth Sciences, University of Geneva, 13 Rue des Maraîchers, 1205 Geneva, Switzerland (corresponding author: branimir.segvic@unige.ch)

Key words: Tunnel valley, smectitization, illite-smectite, diagenesis, Southern North Sea, proglacial lake, Middle Pleistocene

Pre-publication article

Abstract

The Pleistocene sediment infill of elongated glacial incisions of the Southern North Sea (SNS) often is referred to as tunnel valleys (TV). Its depositional environment is not yet fully understood and present study addresses this challenge from a perspective of clay mineral transformation (illite to I-S) reported from the largest Elsterian TV of SNS. Material acquired from the K14-12 borehole in the Dutch offshore was analyzed by X-ray diffraction, electron microscopy, electron microprobe analyses, and laser particle-size analysis. Illite and illite-smectite appeared as dominant clays along with minor amounts of kaolinite, kaolinite-smectite, and chlorite. Highest amount of I-S is recognized in TV main portion, while in pre-glacial and uppermost deposits I-S is less abundant. The XRD peak fitting and deconvolution suggest I-S consists of several intermediates – ordered (well-crystallized illite + R3 I-S) and disordered (R0 I-S + R0 I-SS). Given the average particle sizes (> 2 µm) and Kübler index values (0.415-0.341°$\Delta 2\theta$), illite as well as chlorite and kaolinite were interpreted as detrital. On the basis of I-S distinctive distribution, grain sizes, and compositional variations its formation by way of early diagenetic *in-situ* smectitization of illite under a cold climate is proposed. The process operated via a series of mixed-layer intermediates derived from an illite component being progressively converted to low-charged smectite. The reaction is marked by a significant net loss of K and Al with replacement by Si in a tetrahedral coordination. Layer charge imbalance is accommodated by Fe^{3+} and Mg entering an octahedral layer, whereas Ca partly fills the interlayer sites. Smectitization rates were controlled by illite grain sizes. The results of this study strongly support the existence of an ice-marginal fresh water depositional environment at the glacial maximum in SNS in which early diagenesis at low temperatures resulted in incomplete illite conversion into smectite.

This is a 'pre-publication' version of an accepted article for Clays and Clay Minerals.
This version may be subject to change during the production process.
The DOI given, which may be used for citation purposes, though which will not be active until the version of record is published, is DOI: 10.1346/CCMN.2016.064026

INTRODUCTION AND GEOLOGICAL SETTING

A large number of elongated glacial incisions known as "tunnel valleys" formed under subglacial conditions at former ice-margins of the Quaternary ice-sheets (Figure 1**;** Laban, 1995; Praeg, 1996; Huuse and Lykke-Andersen, 2000; Kehew *et al.*, 2012; Moreau *et al.*, 2012; van der Vegt *et al.*, 2012), which repeatedly occupied the North Sea over the last 1 million years (Huuse and Lykke-Andersen, 2000; Ehlers and Gibbard, 2004). The largest and deepest tunnel valleys in the Southern North Sea (SNS, Figure 2a) are generally referred to the Elsterian glaciation (dating MIS 12 − 480-420 ka according to Cohen and Gibbard (2010); MIS 10 − 390-340 ka according to Lee *et al.* (2012)), when British and Scandinavian ice-sheets covered the majority of SNS (*e.g.* Mangerud and Jansen, 1996). Most of the SNS tunnel valleys (TV) share common clinoform sandy-silty-clayey infill (Figure 2b) thought to present either a reworked preglacial or the newly brought Quaternary sediments (Praeg, 1996). The focus of this study are the sediments of the largest Elsterian TV of the SNS (Figure 2), in particular the mineralogy and geochemistry of clay minerals content, crucial for a better understanding of depositional paleoenvironments and early diagenetic processes involved in the clay mineral formation.

During the biggest part of Tertiary and Quaternary the area of Southern North Sea was exposed to the shallow marine sedimentation in which fine to medium-grained sands prevailed (de Gans, 2007; de Lugt, 2007). Diversity of clay mineral assemblages found in those sands reflected at the time dominant fluvial systems that brought large amounts of sediments mainly from east (Baltic, Scandinavia, Eastern Germany) and south (Central Europe) (Zagwijn, 1989; de Gans, 2007; Westerhoff, 2009). The easterly sourced material was transported by the Baltic River System (BRS, Figure 1; Bijlsma, 1981; de Gans, 2007), which gave rise to the progressive filling of the whole SNS basin with sediments enriched in illite and kaolinite, and depleted in smectite during the Late Pliocene and the Early Pleistocene (Leipe and Sea, 2003; Kuhlmann *et al.*, 2004; Nielsen *et al.*, 2015). In contrast, the fine-grained sediment enriched in smectite was largely supplied by European rivers (Kuhlmann *et al.*, 2004; Adriaens, 2015; Griffioen *et al.*, 2016). Those became important in the Dutch SNS only by the upper Early Pleistocene when the BRS slowly ceased its activity (Zagwijn, 1989; de Gans, 2007; Westerhoff, 2009). Generally speaking, the Quaternary deposits of the Southern North Sea present a

This is a 'pre-publication' version of an accepted article for Clays and Clay Minerals.
This version may be subject to change during the production process.
The DOI given, which may be used for citation purposes, though which will not be active until the version of record is published, is DOI: 10.1346/CCMN.2016.064026

mixture of many different sources and are dominated by illite and smectite along with their mixed-layer phases while kaolinite and chlorite are less abundant (Griffioen *et al.*, 2016 and references therein). However, in the fine fraction of analyzed TV sediments illite and illite-rich I-S (Sme content ≤ 31%) have been reported as the most common phases. Such a finding corresponds only partly to the existing literature data due to complete lack of discrete smectite and scarcity on Sme-rich mixed-layer clays (Sme content > 50 %; Irion and Zöllmer, 1999; Zuther *et al.*, 2000; Huggett and Knox, 2006; Adriaens, 2015; Griffioen *et al.*, 2016). Hence, the clays of the Elsterian TV investigated in this study are presumably linked to the glacially reworked, smectite-free, material brought by BRS and deposited in the area of SNS during the Early Pleistocene. Although I-S mixed-layer minerals are not uncommon for Quaternary deposits of cold latitudinal zones, their peculiar distribution in the analyzed sedimentary succession and distinct mineralogical and geochemical characteristics put forth a possibility of diagenetic *in-situ* origin of smectite mixed-layering (i.e. smectitization of illite). The deep sediment burial usually held responsible for I-S formation through the illitization of smectite (Chamley, 1989) cannot explain the origin of I-S from studied sediments due to the shallow burial history of the deposits, which have never experienced a burial depth greater than 550 m. Therefore, the purpose of this study was to frame and test the hypothesis that reaction of detrital illite with cold fresh water in a glaciolacustrine meltwater paleoenvironment produced early diagenetic mixed-layer I-S. Mineral transformations of this type are usually referred to as *degradation* and are characteristic of continental weathering (Thorez, 1989), rarely taking place during sedimentation and diagenesis (Millot, 1971). In the latter case the sediment must have been exposed to percolating solution able to degrade clay minerals, which is the process only sporadically reported in the literature (Smoot, 1960). This paper provides the first evidences on early diagenetic transformation of illite into I-S in the Quaternary sediments of the North Sea, within the peculiar glaciogenic microenvironment of tunnel valleys, where meltwater played a role of degrading fluids. Clay mineralogy thus provided new constraints on the mechanism of TV formation and sediment filling, which may be of global importance as TVs are still being formed at the margins of continental ice sheets and the fine fraction of their sedimentary infill is seriously under-researched (*e.g.* Kehew *et al.*, 2012). The fresh-water hydrologic system advocated in this research as indispensable for illite transformation into

This is a 'pre-publication' version of an accepted article for Clays and Clay Minerals.
This version may be subject to change during the production process.
The DOI given, which may be used for citation purposes, though which will not be active until the version of record is published, is DOI: 10.1346/CCMN.2016.064026

intermediate I-S is discussed further on in light of Pleistocene proglacial lake debate. Such a lake has been previously suggested to exist at the southern margin of the ice-sheet in an area comprising Benelux and the uncovered part of the Southern North Sea (Figure 1; *e.g.* Gibbard, 2007; Gupta *et al.*, 2007; Murton and Murton, 2012).

STRATIGRAPHIC CONTEXT AND DESCRIPTION OF SAMPLED MATERIAL

The Elsterian tunnel valley investigated in this study represents the largest such feature currently known in the SNS (Moreau *et al.*, 2012). The valley is an elongated north-south depression 100 km in length, 2-3 km in width, and up to 500 m in depth (Benvenuti and Moscariello, 2016). The tunnel valley is filled with a thick succession of deposits that appear as three different units on seismic sections: a lower northward dipping clinoform-dominated unit (Unit A), an upper horizontal layered unit (Unit B) and a unit characterized by chaotic seismic facies (Unit C) (Figure 2b; Benvenuti and Moscariello, 2016). Sediment samples (ditch cuttings) from the borehole K14-12 located in the K block of the Dutch offshore were provided by Nederlandse Aardolie Maatschappij (Shell) (Figure 2). For the purpose of this research, 36 sediment samples were collected at 10 m intervals. Drilling mud consisted of sea water bentonite and carboxymethylcellulose (CMC) mud (Shell, 1993), with minimal influence on sample mineralogy as indicate by the near-complete absence of discrete smectite agglomerations.

Samples cover a measured depth (MD) interval along the borehole of 550 to 200 m and are named after their position along the borehole. Those from between 550 and 500 m define the pre-glacial sediments below the tunnel valley floor (Benvenuti and Moscariello, 2016). In the study area, Harding (2015) showed the presence of a thick package of sediments dating from Lower Early Pleistocene at the depths investigated in this research. The tunnel valley floor is identified at 500 m. Samples from the 490 to 280 m range represent the northward-dipping clinoform unit (Unit A). Samples from between 270 and 240 m are from the unit dominated by horizontal layers (Unit B). Samples from 230 m sample the chaotic unit that is poorly characterized, given the inadequate seismic data quality in shallow intervals (Unit C). QEMSCAN® investigation was performed on the entire range of samples, while seven samples were selected to study the clay fraction in detail.

This is a 'pre-publication' version of an accepted article for Clays and Clay Minerals.
This version may be subject to change during the production process.
The DOI given, which may be used for citation purposes, though which will not be active until the version of record is published, is DOI: 10.1346/CCMN.2016.064026

ANALYTICAL METHODS

Grain size analysis

All 36 sediment cutting samples were sieved using a two-step sieving procedure. First, wet sieving was performed on 30 g of dry, loose material. Sieves ranged from 0.063 to 2 mm on a φ - scale based succession. Following a complete drying, each sample and every size class of the material were weighed. The material finer than 0.063 mm was analyzed using a laser particle size analyzer CILAS 1180 (CILAS, Orléans, France) installed at the Department of Earth Sciences (University of Geneva, Switzerland). Coarse particles were measured using a real-time fast Fourier transform of the image obtained with a charge coupled device camera equipped with a digital processing unit. The results on particle sizes were recovered in vol% and were later converted to grams to conform to the overall dataset obtained by manual sieving. The data were treated with the GRADSTAT software (Blott and Pye, 2001) yielding the results displayed as percentages of the respective grain size classes and as averages (Folk and Ward, 1957).

QEMSCAN® and SEM clay morphology study

In order to produce thin sections used for the microbeam investigations (QEMSCAN®, SEM-EDS, EMPA) the rock chips were mounted to the glass substrate using the ARA XW 396 epoxy resin combined with the ARA XW 397 hardener, respecting a 10:3 weight ratio. The injection of resin was completed under the vacuum and thin sections produced thereupon were dried for 12 hours at 50 °C. Automated mineral and textural characterization was performed using a FEI QEMSCAN® Quanta 650F facility (FEI Company, Oregon, USA). This system featured by the field emission gun (FEG) electron source is installed at the Department of Earth Sciences (University of Geneva, Switzerland). Mineral phase identification relies on the combination of back-scattered electron (BSE) contrast and EDS spectra giving information on the elemental composition (Gottlieb *et al.*, 2000). Individual X-ray spectra were compared to a library of known spectra and a mineral name was assigned to each individual acquisition point. The X-ray EDS spectra library, initially provided by the manufacturer, has been further developed in-house using a variety of natural standards. Measurements were

This is a 'pre-publication' version of an accepted article for Clays and Clay Minerals.
This version may be subject to change during the production process.
The DOI given, which may be used for citation purposes, though which will not be active until the version of record is published, is DOI: 10.1346/CCMN.2016.064026

146 performed on carbon-coated thin sections that were minimally polished in order to avoid a clay
147 fraction loss. Analytical conditions included a high vacuum and an acceleration voltage of 15 kV with
148 probe current of 10 nA. X-ray acquisition time was 10 ms per pixel using a point-spacing of 2.5 µm.
149 Up to 122 individual fields of view were measured in each sample, with 1.5 mm per single field.
150 Gold-coated thin sections were used for SEM investigations. Crystal morphology, shapes, and
151 mineral agglomerations were studied by high-magnification back-scattered electron (BSE) and
152 secondary electron (SE) imaging using QEMSCAN® facility operated in SEM mode under high
153 vacuum. A variety of acceleration voltages and beam size conditions were employed to assure the best
154 imaging conditions.
155
156 *XRD mineralogy*
157 X-ray powder diffraction was performed on whole-rocks samples, as well as the clay fraction.
158 Sample preparation initially included material powdering in an agate mortar prior to whole-rock
159 measurements. Seven representative samples, covering the whole stratigraphic section investigated,
160 were chosen for further investigations on clay mineral fraction (Figure 2c). To prevent possible mixing
161 of detrital with authigenic clays, the samples were not powdered but only gently disaggregated. The
162 clay fraction was separated from the crushed material by centrifugation, which first involved the
163 removal of organic matter using 10 wt% H_2O_2 for at least 24 h. Na-metaphosphate was added to
164 disperse the clays. Further disaggregation was accomplished in an ultrasonic bath. To ensure a uniform
165 cation exchange, clay fractions separated by centrifugation were saturated by Mg using a solution of
166 10 ml of approximately 4M $MgCl_2$. Suspensions were washed and centrifuged with distilled water at
167 least three times to minimize the content of free ions. The oriented mounts were prepared using a
168 Millipore membrane filter and a vacuum filtration device. After the clay suspension was drawn onto
169 the filter, it was left to dry at 50°C prior to the transfer to porous ceramic tiles. The thickness of such
170 prepared mounts exceeded 50 µm, which is required for semi-quantitative determination of the clay
171 mineral content (*e.g.* 'infinite thickness' of Moore and Reynolds, 1997). The rest of the clay-fraction
172 material was used for laser particle size analysis by means of the laser particle size analyzer method
173 described above (CILAS 1180).

This is a 'pre-publication' version of an accepted article for Clays and Clay Minerals.
This version may be subject to change during the production process.
The DOI given, which may be used for citation purposes, though which will not be active until the version of record is published, is DOI: 10.1346/CCMN.2016.064026

The measurements were undertaken in air-dried (AD) conditions, after ethylene-glycol (EG) saturation, and after heating for 1 h at 300°C. The BRUKER D8 Advance diffractometer (BRUKER AXS GmbH, Karlsruhe, Germany) installed at the Department of Physics (University of Geneva, Switzerland) was used for XRD analyses. This instrument features a horizontal goniometer axis and synchronized rotation of both the X-ray source and the detector arms. The sizes of the divergent and the receiving slits were 1° and 0.1 mm, respectively. Measurement parameters comprised a continuous scan in the Bragg-Brentano geometry using Cu$K\alpha$ radiation (45 kV and 44 mA) with curved-graphite monochromator. At a counting time of 370s per 0.012° sample mounts were scanned from 3 to 70° and 3 to 30°2θ for whole-rock and clay-fraction, respectively.

Electron microprobe analyses

Electron microprobe analyses and elemental X-ray study were carried out by using the JEOL JXA 8200 Superprobe wavelength/energy dispersive (JEOL Ltd., Akishima, Japan) combined microanalyzer installed at the Institute of Earth Sciences (University of Lausanne, Switzerland). Operating parameters included an accelerating voltage of 20 kV, a 20 nA beam current, and a 1 μm beam size. Counting times of 20 s on peak and 10 s on background on both sides of the peak were used for all elements. Limits of detection (LOD) were calculated as the minimum concentration required to produce count rates three times higher than the square root of the background (3 σ; 99 wt% degree of confidence at the lowest detection limit). Concentrations below LOD are reported as not detected. Raw data were corrected for matrix effects using the PAP algorithm implemented by JEOL (Pouchou and Pichoir, 1984, 1985). Natural minerals, oxides (corundum, spinel, hematite, and rutile), and silicates (albite, orthoclase, anorthite, and wollastonite) were used for calibration. Mineral formulae were calculated using a software package designed by H-P. Meyer (University of Heidelberg, Germany). For the calculation of illite and mica formulas, all Fe was assumed to be ferric. Iron, Mg, and Ti were assumed to be octahedral, while Al was assumed to be tetrahedral up to Si + Al = four atoms per 11 oxygens, with remaining Al assigned to octahedral sites. For mixed-layer minerals containing smectite (I-S and I-SS), the totals of measured elements ranged between 70.01 and 82.92

This is a 'pre-publication' version of an accepted article for Clays and Clay Minerals.
This version may be subject to change during the production process.
The DOI given, which may be used for citation purposes, though which will not be active until the version of record is published, is DOI: 10.1346/CCMN.2016.064026

wt%, thus reflecting (1) the difference in smectite component abundances, (2) high amounts of water in the smectite component, (3) and the potential porosity between clay particles.

Interpretation and modelling of XRD patterns

The mineral phases were identified using the Powder Diffraction File (1996) data system and the *Panalytical© HighScore Plus (v. 3.0e)* program package (PANalytical, Almelo, The Netherlands). X-ray diffraction patterns of clay minerals were examined using methods described by Moore and Reynolds (1997) and Środoń (2006). For chlorite mineral interpretation, the recommendations of Lagaly *et al.* (2006) and Meunier (2007) were followed. Illite crystallinity values, in recent years better known as the Kübler index (KI: Kubler, 1964; Guggenheim *et al.*, 2002), are defined by the width of the illite 001 peak measured at half of the peak height above the background (Eberl and Velde, 1989) were measured using the *Panalytical© X'pert data viewer*. Expressed as $°\Delta 2\theta$, KI values were used to characterize the environment of illite formation, taking into account that diagenetic illite has KI values > $0.42°\Delta 2\theta$, whereas the range of KI values from 0.30 to $0.42°\Delta 2\theta$ corresponds to low metamorphic anchizone, from 0.25 to $0.30°\Delta 2\theta$ is the high anchizone and KI < $0.25°\Delta 2\theta$ defines the metamorphic epizone (*e.g.* Kemp and Merriman, 2009). The calibration of KI values was carried out using the international standards provided by Warr and Rice (1994). Characterizing mixed layering only by analyzing the 001/002 and 002/003 I-S peak positions was practically impossible given the fact that analyzed samples were composed of detrital illite and I-S mixed−layer minerals both rich and poor in illite (Moore and Reynolds, 1997). To characterize the mixed−layer clay minerals, XRD clay fraction patterns were therefore modelled using Sybilla© software (property of Chevron™, San Ramon, California, USA) based on the formalism of Drits and Sakharov (1976). The modelling included a trial-and-error procedure that provided optimal clay mineral structural and probability parameters to get the best fit between experimental and calculated patterns, and intensities of 00*l* reflections for each of the clay phases present. For mixed−layer minerals the number, nature, and stacking sequence of different compositional layers were taken as modifiable values (*e.g.* Uzarowicz *et al.*, 2012). To produce the experimental spectra, three discrete phases were introduced (illite, chlorite,

This is a 'pre-publication' version of an accepted article for Clays and Clay Minerals.
This version may be subject to change during the production process.
The DOI given, which may be used for citation purposes, though which will not be active until the version of record is published, is DOI: 10.1346/CCMN.2016.064026

and kaolinite). R3 I-S, a mixed−layer illite-smectite with long-range ordering (Reichweit > 1) was introduced to accommodate the 001 peak asymmetry of illite at lower 2θ values. Higher background values between the 001 peaks of chlorite and illite were modelled by addition of R0 I-S and R0 I-SS, low ordered (Reichweit = 0) illite-smectites with one smectite layer with two water molecules and two smectite layers with one and two water molecules. R0 I-SSS was further introduced to mimic the illite-smectite short range polytypes in which the 001* superstructure diffraction peak was found in a range of 22-25 Å (Velde, 1985), thus accommodating an intensity increase reported around 5°2θ. An additional mixed−layer phase, kaolinite-smectite (K-S), was used as well, fitting the low-angle shoulder at the kaolinite basal diffraction peak. The R0 variety was used as most of documented K-S occurrences were found to be randomly stratified (*e.g.* Dudek *et al.*, 2006). Modelling parameters of mixed−layer minerals consisted of (1) the orientations of particles on the mounted X-ray slides (σ*), (2) coherent scattering domain sizes expressed in number of layers (CSDS), and (3) the amounts of smectite component (Sme) in mixed−layer phases (Table 1). The relative clay mineral content was determined using the integrated peak area values of illite (002), kaolinite (002), and chlorite (003) weighted by appropriate mineral reference intensities and normalized (Moore and Reynolds, 1997). The relative abundance of clay minerals was therefore refined using Sybilla© modelling, allowing the amounts of smectite layers present in mixed−layer clay phases to be estimated. Clay mineral nomenclature followed the AIPEA recommendations with the terms smectite, illite, kaolinite, and chlorite used as general expressions for the respective mineral groups (Bailey, 1980).

A decomposition of the air-dried XRD patterns was performed using DecompXR software (Lanson, 1993). The area modelled ranged from 5 to 10°2θ where, depending on the composition of mixed-layer I-S, its first basal diffraction peak is located. Having subtracted the background, experimental patterns were decomposed by six Gaussian elementary curves representing mineral compounds used for Sybilla modelling (illite, chlorite, R3 I-S, R0 I-S, R0 I-SS, and R0 I-SSS). All the compounds met the criteria of Lanson and Besson (1992) requiring the elemental curves to have a minimum peak position and width difference of 0.3 and 0.2°2θ, respectively.

This is a 'pre-publication' version of an accepted article for Clays and Clay Minerals.
This version may be subject to change during the production process.
The DOI given, which may be used for citation purposes, though which will not be active until the version of record is published, is DOI: 10.1346/CCMN.2016.064026

Statistical analyses

Multivariate statistical analysis, specifically principal component analysis (PCA), was performed on seven samples to identify the principal components that control variations in mineralogical abundances and the relationship between mineral phases and grain size classes. The analysis was conducted on mineral compositional data of the fine fraction as determined after the modelling of the XRD patterns. The centered log-ratio transformation (Aitchinson, 1982) was applied to the compositional data in order to remove the non-negativity and constant-sum constraints typical of compositional variables. The PCA analysis was conducted by 'R' software ("R core team", New Zealand) using the package FactoMineR (Lê *et al.*, 2008). Grain size data, expressed in volume of material per grain size classes, were used in line with the mineral composition data as quantitative supplementary variables.

RESULTS

Grain-size and bulk-rock mineralogy

The lower parts of the analyzed Elsterian tunnel valley (Unit A, Figure 2c) contain sediments dominated by medium to coarse sand with the mean (after Folk and Ward, 1957) grain size of approximately 500 µm. Higher in the succession, the grain size became progressively finer, reaching 20 wt% clay in the upper portions of Unit A (TV infill), as well as Units B and C. In Units B and C the abundance of sand was less than 10 wt%, with a mean particle size of about 10 µm and less. The pre-glacial sediments below the Elsterian tunnel valley are characterized by a clear bimodal character having practically equal amounts of gravel and sandy grains versus clay and fine silt particles. The mean grain size was in the medium silt range (~50 µm) although the bimodal size distribution means that this mean is not amply represented in the sediments.

The modal mineralogy was clearly controlled by variations in the grain size up the stratigraphical section (Figure 2c). Quartz is most abundant in the lower portions of Unit A, where sediment is the coarsest. In contrast, in the fine-grained portion of the section (*i.e.* the uppermost stratigraphic interval) the highly-crystalline illite was the dominant phase; elsewhere it was the second most

This is a 'pre-publication' version of an accepted article for Clays and Clay Minerals.
This version may be subject to change during the production process.
The DOI given, which may be used for citation purposes, though which will not be active until the version of record is published, is DOI: 10.1346/CCMN.2016.064026

abundant component. Especially illustrative is the illite/quartz ratio, being practically inversely proportional to the mean grain size curve (Figure 2c), thus suggesting quartz and illite dominated the coarse and fine fraction, respectively. Feldspars, generally albitic, constituted <10 wt%. Biotite and muscovite, up to several mm in grain size, are widespread but in relatively low amounts (~3 wt%).The carbonate minerals, calcite and aragonite, were abundant in the coarse fraction, occurring exclusively as bioclasts. Agglomerates of detrital grains coated by a pyritic and/or sideritic matrix were abundant in the pre-glacial deposits, while they were less abundant in the TV infill, and increased in abundance in the Units B and C. The coarse size of bioclasts and diagenetic minerals caused a bimodality of the grain size curve of the pre-glacial deposits as well as in some samples of Units B and C (Figure 2c). Clay minerals other than illite (*i.e.* kaolinite, chlorite) were detected by QEMSCAN® and XRD whole-rock measurements only in low amounts (~0.5-1 wt%, 2-3 wt%, respectively; Table 2). Discrete smectite was not detected by XRD measurements, while in the QEMSCAN® analyses smectite occurred in very low amounts (<0.2 wt%, Table 2).

Clay mineralogy and SEM characterization of clayey particles

An assemblage consisting of illite, illite-smectite, kaolinite, and chlorite characterized the clay fraction (Figure 3). The summed abundances of illite and various mixed-layer illite-smectites varied between 63 wt% in pre-glacial deposits (sample 530) and 80 wt% in Unit C (sample 220, Table 3). The amounts of chlorite and kaolinite (including K-S) were between 5-8 wt% and 15-30 wt%, respectively (Table 3). The abundances of kaolinite were inversely proportional to those of illite and illitic minerals, with the highest amounts of the former and lowest of the latter recorded in pre-glacial deposits, whereas in the post-glacial layers the ratio was inverse (Table 3). Low percentages of non-clay minerals were also detected in all the analyzed samples (quartz and feldspar, Figure 3), but these were not taken into account during quantification. Based on the analysis of the X-ray diffraction patterns and the results of spectra modelling and study of particle morphologies, the following detailed characterization of clay minerals was prepared.

Illite – Illite was defined by the sequence of basal 00l diffraction peaks that were not affected by glycolation (Figure 3, EG curves). Relying on the profile fitting and deconvolution (Figures 4-5), illite

This is a 'pre-publication' version of an accepted article for Clays and Clay Minerals.
This version may be subject to change during the production process.
The DOI given, which may be used for citation purposes, though which will not be active until the version of record is published, is DOI: 10.1346/CCMN.2016.064026

comprised two non-expandable phases between d_{001} 9.96-10.01 (illite sensu stricto) and d_{001} 10.08-10.14 Å (R3 I-S), with less than 5 and 13 wt% smectite layers, respectively (Table 1). In general, the 001 peaks of illite are relatively broad with illite KI values ranging from 0.415 (sample 240) to 0.341°$\Delta 2\theta$ (sample 310). The SEM-EDS investigation revealed illite forming irregular flake-like platelets oriented parallel to each other (Figure 6a). Illite sparsely occurs in a rod-like form (Figure 6b). In either case, relations between XRD mineralogy and particle grain sizes revealed the size of illite particles to be in a range of several microns (Figure 7a). Somewhat larger particles (~10-15 μm) were probably muscovite (Figure 6a) or biotite (Figures 6b).

Mixed-layer illite-smectite – Expandable interstratifications of illite and smectite were identified as mixed-layer I-S and were first identified visually using the criteria of Reynolds and Hower (1970) due to a broad diffraction peak at ~17 Å appearing in EG samples (Figure 3). More light on the nature of I-S was provided by pattern fitting which revealed the presence of two disordered smectite-rich mixed-layer I-S (R0 I-S, R0 I-SS, Table 1) that accompanied a disordered R0 K-S and ordered R3 I-S (Table 1). These four mixed-layer minerals fitted the experimental spectra well (Figure 4). XRD pattern deconvolution preformed after Lanson and Velde (1992) on asymmetric 10 Å bands showed R0 I-S at d_{001} 10.77-10.81 Å and R0 I-SS at d_{001} 13.72-13.80 Å (Figure 5). Both disordered I-S had wide peaks indicating small crystallite thicknesses that continued to diminish as the amount of smectite layers increased. The smectite content was estimated to be between 20-31 and 75-94 wt% for R0 I-S and R0 I-SS, respectively (Table 1). The R0 I-SSS is a curve with no actual meaning used to mimic the superstructure 001^* diffraction peak of disordered I-S found in a range of 22-25 Å (Velde, 1985), also partly affected by the incident X-ray beam (*e.g.* Allmann, 2003). The SEM-EDS showed I-S particles with a flaky morphology that is analogous to that of presumably discrete illite with comparatively smaller particle sizes in a micron range (Figures 6a, 6b, 7b). Occasionally, I-S is reported forming coarser agglomerates having several microns in size (Figure 6c). Mixed-layer phases formed the largest portion of the sample matrix (Figure 6b). Taking into account the Ca content, as well as the octahedral Fe/Mg and in particular tetrahedral Al/Si ratios, the SEM-EDS investigations allowed a quick identification of disordered (smectite-rich) I-S varieties (Welton, 1984), which was further corroborated by EMPA measurements on several representative sample portions.

This is a 'pre-publication' version of an accepted article for Clays and Clay Minerals.
This version may be subject to change during the production process.
The DOI given, which may be used for citation purposes, though which will not be active until the version of record is published, is DOI: 10.1346/CCMN.2016.064026

Chlorite – Despite the fact that the basal peaks of chlorite partly overlapped with kaolinite, chlorite was defined by its d_{002} and d_{004} diffraction peaks at 7.12 and 3.55 Å, respectively (Figures 3-4). Its weak odd-order diffraction peaks were highly pronounced when the 001 diffraction peak was reported to be strongly attenuated. This indicates high Fe abundances in the chlorite structure (Moore and Reynolds, 1997). Using the intensity ratios I(003)/I(005) (Brown and Brindley, 1980) and profile fitting, the total content of Fe in chlorite was found to be ~2.34 a.p.f.u., which corresponds well to the Fe concentration in chlorite determined by EMPA (2.19 a.p.f.u., Table 4). A heating treatment at 300ºC showed no evidence of a partly expandable vermiculite-type phase of 14 Å was present. In SEM-EDS, chlorite appeared either as relatively coarse detrital grains (up to 50 μm in size, Figure 6b) or replacing crystallites of biotite (Figure 6d). No significant differences in the crystal chemistry between the two chlorite habits were documented.

Kaolinite and mixed-layer kaolinite-smectite – The diffraction peaks at ~7.22 (d_{001}) and 3.63 Å (d_{002}) were diagnostic for kaolinite presence in analyzed sediment. Although relatively well defined and symmetrical, the kaolinite second basal diffraction peak showed a tailing in the low angle region (Figures 3-4), suggesting the presence of minor interstratified 2:1 clay minerals, presumably smectite (*e.g.* Dudek *et al.*, 2006; Hong *et al.*, 2012). The EG solvation showed an increase of the d_{001} peak of kaolinite, while the low-angle shoulder migrated towards higher d values. The shift of the tailing that takes place after glycolation, from about 7.4 to 7.8 Å, is normally considered as an evidence of smectite interlayering (Schultz *et al.*, 1971). Hence, apart from the kaolinite d_{001} diffraction peak to fit XRD spectra (Figure 4) a disordered R0 K-S with a maximum at ~7.4 Å and up to 7 wt% of the smectite component (Table 1) was used. Kaolinite particles are well-dispersed within the illite-dominated matrix, forming aggregates with sizes from 10 to 20 μm devoid of characteristic shapes (Figure 6b).

Mineral phase chemistry

The representative mineral chemistry of selected clay minerals from the SNS sediment are reported along with few analyses of coarser mica and kaolinite that served for a reference (Table 4). The composition of *chlorite* is characterized by a total cation content slightly below 10, suggesting a

This is a 'pre-publication' version of an accepted article for Clays and Clay Minerals.
This version may be subject to change during the production process.
The DOI given, which may be used for citation purposes, though which will not be active until the version of record is published, is DOI: 10.1346/CCMN.2016.064026

dominance of divalent Fe, resulting in the classification of the chlorites as trioctahedral. Accordingly, the chlorite may be defined as pycnochlorite (X_{Fe} = 51) (Hey, 1954). The *kaolinite* composition is non-stoichiometric given the Si depletion (2.83-3.04 a.p.f.u.) and Fe enrichment (0.15-0.21 a.p.f.u.), respectively. This may be attributed to the development of porosity between packets of kaolinite, the presence of micron-scale impurities in form of Fe-Ti bearing minerals, or smectite interlayering (*e.g.* Cuadros and Altaner, 1998; Sengupta *et al.*, 2008). Regardless of the variable valence of Fe, the total octahedral cation content of *mica* was below 2.5 a.p.f.u. (2.03-2.04 and 2.41-2.47 for muscovite and biotite, respectively), which, according to Rieder *et al.* (1998), defined them as dioctahedral mica. The biotite composition covers the fields between $1.614 \leq (Al^{IV} + Al^{VI}) \leq 1.750$ a.p.f.u., while for muscovite the $(Al^{IV} + Al^{VI})$ ranged between 2.549 and 2.805 a.p.f.u. Both micas are characterized by variable levels of Mg, Fe, and Ti substituting for octahedral Al (phengite substitution). K-rich white mica referred here as 'muscovite' is of phengitic composition (Si ≥ 3.1 a.p.f.u., Rieder *et al.*, 1998). The average phase chemistry of *illites* (illite sensu stricto, R3 I-S) and *mixed-layer illite-smectite* (R0 I-S, R0 I-SS) is $(Ca_{0.034}K_{0.451}Na_{0.117})(Al_{1.548}Fe^{3+}_{0.253}Mg_{0.249}Ti_{0.023})^{VI}(Si_{3.366}Al_{0.634})^{IV}O_{10}[(OH)_2,(H_2O)]$ (16 analyses) and $(Ca_{0.102}K_{0.332}Na_{0.136})(Al_{1.336}Fe^{3+}_{0.386}Mg_{0.326}Ti_{0.031})^{VI}(Si_{3.377}Al_{0.623})^{IV}O_{10}(OH)_2 \cdot nH_2O$ (45 analyses), respectively. In the EMPA data presentation, all the mixed-layer I-S species used for XRD profile fitting were arbitrarily referred to mixed-layer I-S. As reported by Norrish and Pickering (1983), the K_2O content in illite-like phases is inversely related to that of H_2O (Table 4). When comparing illite and interstratified I-S, the latter is characterized by an elevated content of Ca, up to 0.169 Ca p.f.u. In the case of K, an inverse trend was reported, with I-S rich in Ca being depleted in K content (Figures 8a). A similar distinction was inferred from the occupancy of tetrahedral and octahedral sites (Figure 8b), with illite showing a comparatively higher Al^{IV} (hence lower Si, Table 4), whereas mixed-layer minerals were characterized by elevated abundances of octahedral Fe and Mg. For those I-S featured by the highest proportions of octahedral Fe and Mg (samples 310 and 350, Table 4) part of Mg was allocated into the interlayer structural position in order to respect the maximal cation occupancy per octahedral layer. Such peculiar phase chemistry can be explained by restricted chlorite interlayering (~10%), which give rise to the formation of mixed-layer illite-chlorite-smectite clays (Weaver and Beck, 1971). Somewhat higher water contents documented in I-S from samples 310

This is a 'pre-publication' version of an accepted article for Clays and Clay Minerals.
This version may be subject to change during the production process.
The DOI given, which may be used for citation purposes, though which will not be active until the version of record is published, is DOI: 10.1346/CCMN.2016.064026

394 and 350 (Table 4) conform to this line of reasoning. Regarding the compositions of pure smectites and
395 nearly pure smectites (I-S with more than 80 wt% of Sme, Boles and Franks (1979) Ramseyer and
396 Boles (1986) and references therein) and that of illites with less than 10 wt% of the Sme component
397 (Deer *et al.*, 1996; Meunier and Velde, 2004), the illites and I-S analyzed in this study are projected in
398 the lower segment of the illite compositional field, while some of the I-S analyses approached the
399 composition of smectite-rich I(0.2)-S(0.8) (Figure 8b). The mixed-layer smectite component is defined
400 as dioctahedral and close to beidellite in composition (Table 4; Grim, 1968).
401
402 *Clay mineral distribution*
403 The clay mineral investigation of sediments from borehole K14-12 in the Dutch North Sea showed
404 illite and kaolinite as well as their smectite interstratifications as dominant clay phases (illite sensu
405 stricto + R3 I-S 34-52 wt%; illite-smectite (R0 I-S, R0 I-SS) 22-41 wt%; kaolinite 7-10 wt%;
406 kaolinite-smectite 7-20 wt%; Table 3). The highest amounts of illite (illite and R3 I-S) were recorded
407 in the overlying unit (sample 220) with slightly lower amounts in Unit B (sample 240) and in the pre-
408 glacial deposits (sample 530; Figure 7). These values coincided with the lowest amounts of I-S and,
409 consequently, with the lowest proportions of the total smectite component (Sme_{TOT} - sum of smectite
410 layers from all I-S present, Table 3). Unit A, representing the clinoform tunnel valley infill (samples
411 310, 350, 370, and 440) was characterized by lower illite abundances coupled with elevated I-S and
412 Sme_{TOT}. The latter is, thus, inferred to have maximal concentrations in the central portions of the TV
413 infill (samples 350 and 370 with 20 and 18 wt% Sme_{TOT}, respectively, Table 3; Figure 2c). In contrast,
414 the kaolinite (kaolinite + R0 K-S) content is the highest in pre-glacial sediments, whereas in the TV
415 succession it maintained a uniform content at about 20 wt%, except in the uppermost unit where it was
416 even lower (Table 3).
417
418 **DISCUSSION**
419 The area of the Southern North Sea offers an opportunity to investigate the provenance and
420 'source-to-sink' transport of terrigenous material in a marginal sea (*e.g.* Irion and Zöllmer, 1999;
421 Leipe and Sea, 2003; Kuhlmann *et al.*, 2004; Nielsen *et al.*, 2015; Griffioen *et al.*, 2016). Clay

This is a 'pre-publication' version of an accepted article for Clays and Clay Minerals.
This version may be subject to change during the production process.
The DOI given, which may be used for citation purposes, though which will not be active until the version of record is published, is DOI: 10.1346/CCMN.2016.064026

minerals in particular may serve as effective tools to establish the origin of fine-grained terrigenous sediment. In the area studied, clay minerals consist mainly of illite and mixed-layer illite-smectite with minor kaolinite and chlorite (Table 3). In depositional eogenetic environments, illite as well as kaolinite and chlorite do not form; therefore, when found in sediments that have not suffered deep-burial diagenesis they are considered detrital rather than neoformed (Meunier and Velde, 2004). Illite KI values (0.415 - 0.341°$\Delta 2\theta$), although somewhat compromised by Sme interlayering (R3 I-S with d_{001} 10.08-10.14 Å; Figure 5), provide an additional piece of evidence for the detrital nature of the illite (*e.g.* Ferreiro Mählmann *et al.*, 2012). The size of illite particles (~ 5 - 10 µm, Figure 7a) and its flaky particle structure (Figure 6a) are also features that suggest the detrital origin of the illite (Iacoviello *et al.*, 2012).

The analyzed succession consists of different units characterized by similar mineralogy of the clay fraction. The most striking feature in terms of clay composition is lack of discrete smectite, which suggests little input from central European rivers before and after the Elsterian glaciation (Kuhlmann *et al.*, 2004; Adriaens, 2015; Griffioen *et al.*, 2016). Knowing that in the time of the upper Early Pleistocene the material transport by the BRS practically stopped, the sediment of the TV infill can be considered as glaciogenic, older smectite-free material that was locally eroded during the formation of TV. In the analyzed TV sequence no discrete smectite is observed and illite along with illite-rich I-S are the dominant clay species (Table 3). Within the studied TV sediment section the distribution of smectite-rich I-S (R0 I-S + R0 I-SS, Table 1) was shown to be of particular importance. Namely, I-S displayed maximal abundances in the TV infill (Unit A, Figure 2c), while it appears in significantly lower amounts in the Units B and C, as well as in the pre-glacial deposits (Table 3). The same pattern is inferred for the total smectite content (Sme_{TOT}) calculated from all identified I-S species (Tables 1, 3). Within Unit A it is reported that those horizons that have been exposed to the influence of meltwater for the longest period of time (*i.e.* earliest clinoforms) have the highest Sme_{TOT} values (samples 350-440; Figure 2; Table 3). Such indicative distribution of I-S in sediments of analyzed Elsterian TV along with the known impoverishment of reworked pre-glacial sediments in smectite and I-S put forward the *in-situ* alteration of illite into illite-smectite (*smectitization*) as the most plausible explanation of smectite interlayering in analyzed clays. The process of mineral transformation of

This is a 'pre-publication' version of an accepted article for Clays and Clay Minerals.
This version may be subject to change during the production process.
The DOI given, which may be used for citation purposes, though which will not be active until the version of record is published, is DOI: 10.1346/CCMN.2016.064026

stable clay phases (*i.e.* illite) to open minerals featured by variable basal spacings (*i.e.* I-S) assumes a loss of substance and it is therefore occasionally referred to as degradation (Millot, 1971). Usually such mineral transformation take place in soils and weathering crust affected by degrading fluids (Whittig and Jackson, 1955; Jackson, 1957; Fordham, 1990). In sedimentary environments however the alteration of illite is rarely documented (Smoot, 1960) which is readily explained by restrained matter exchange (Hartmann *et al.*, 1999). Smectitization in analyzed sediments must have occurred by inhibited early chemical diagenesis in a fresh water environment of fluvial or lacustrine nature where meltwater played a role of degrading fluid that percolated through the eroded TV pre-glacial sediment of SNS at glacial maximum when sea-water conditions faded away (de Gans, 2007). Such diagenetic process itself is not isochemical because it requires mobilization of a wide range of elements such as K, Ca, Fe, Mg, and also Al and Si. After the sediment re-deposition within TV, the detrital illite that survived initial weathering and physical erosion reacts with fresh water, giving rise to a range of I-S species (Chamley, 1989 and references therein; Figure 5; Table 3). The smectitization of illite is hypothesized here to have operated in this study area by reaction with cold fresh water by means of a series of mixed-layer intermediates (I-S) with illite being converted to low-charged smectite layers. Most of the total charge remained present within the tetrahedral sheet, even in I-S with highest Sme abundances (Table 4). The first expression of smectitization process was the emergence of ordered R3 I-S with up to 13 wt% of the Sme component (Table 1; Figure 5) as a consequence of an initial decrease of K content from ~0.45 to about 0.35 a.p.f.u. This makes a net loss of about 0.10 a.p.f.u. compared to an average illite composition (Table 4; Figure 8c). At the same time, Si replaces Al in the tetrahedral sheet at an initial compositional difference of ~ 0.005-0.01 a.p.f.u. (Table 4; Figure 8c). Geochemical data do not show released Al to be accommodated in the octahedral sheet of a newly formed smectite component neither is it found building hydroxy interlayers (gibbsite layer) that would eventually lead to the appearance of hydroxy-interlayered smectite (HIS; Meunier, 2007; Table 4; Figure 3). Aluminum was instead leached out from the structure of the newly formed mixed-layer I-S, some it may have been consumed by neoformation of minute crystallites of kaolinite found in sediment matrix. The charge imbalance in I-S caused by the K loss and tetrahedral rearrangements is accommodated by Mg and Fe^{3+} liberated from altered chlorite and biotite (average increase of 0.1 and

This is a 'pre-publication' version of an accepted article for Clays and Clay Minerals.
This version may be subject to change during the production process.
The DOI given, which may be used for citation purposes, though which will not be active until the version of record is published, is DOI: 10.1346/CCMN.2016.064026

0.2 a.p.f.u., respectively; Table 4; Figure 8b). In I-S where highest concentrations of Mg and Fe (> 0.9 a.p.f.u.) are reported (Table 4) part of Mg is accommodated in the interlayer site suggesting a restrained chlorite interlayering in Sme-rich illite-smectite (~10%; Weaver and Beck, 1971). Finally, Ca enters the structure partly filling the interlayer site, such that the I-S is enriched in Ca by ~ 0.02 a.p.f.u. with respect to illite (Table 4; Figure 8a). The retention of Si and Ca in the products of smectitization indicates that these usually easily-leached elements (Schaetzl and Thompson, 2015) were retained in the diagenetic environment. Smaller particles (0.04-0.08 μm; Figure 7a), having comparatively larger reaction surfaces are most likely disordered R0 I-S and R0 I-SS (Table 1; Figure 5), showing advanced smectitization in form of maximal loss of K (~0.25 a.p.f.u.; Table 4; Figure 8c) and minimal Al^{IV} values (~0.55 a.p.f.u.; Table 4). The composition of the octahedral layer, having maximal Fe^{3+} abundances (~0.55 a.p.f.u.; Table 4), approaches I-S compositions with about 80 wt% Sme (Figure 8b; Boles and Franks, 1979; Ramseyer and Boles, 1986), which is consistent with the composition of R0 I-SS defined by XRD modelling to have ~75 – 94 wt% Sme layers (Table 1). An incomplete evolution of illite toward smectite composition may thus be inferred, to be an evolutionary sequence represented by I-S phases of different ordering degree, Sme content, and mineral chemistry.

The smectitization reaction progress is controlled mainly by the particle size of detrital illite, with additional influence by other common factors such as climate, sediment porosity and permeability, and fluid composition (Schaetzl and Thompson, 2015). Based on XRD mineral composition (Table 3) and grain size data, the two principal components that cover about 75% of the total variance in a PCA space define a coherent group of samples belonging to Unit A and, thus, to the peak smectitization, while the samples of pre-glacial and overlying sediments are clearly outliers (Figure 7b; Table 1). The role of the grain size becomes even more apparent in the variable projection plot (Figure 7a), in which the grain size classes are shown as supplementary variables with the finest fraction corresponding to Sme-rich disordered I-S and the coarsest to detrital illite and chlorite. Such a relationship clearly points to larger reaction surfaces of small illite particles that promote smectitization by allowing more fluid-rock interaction, leading to enhanced chemical exchange between solid and fluid phases.

It is proposed here that the formation of mixed-layer I-S described above took place in a fresh water, ice-marginal to proglacial, depositional environment during the glacial maximum. The

This is a 'pre-publication' version of an accepted article for Clays and Clay Minerals.
This version may be subject to change during the production process.
The DOI given, which may be used for citation purposes, though which will not be active until the version of record is published, is DOI: 10.1346/CCMN.2016.064026

progressive ice-sheet withdrawal coeval to sediment accumulation at the ice-margin caused a northwards shift of the depositional environment. Accordingly, the remaining ice-marginal sediments were exposed to the restrained influx of fresh water, in the form of meltwater, as the ice-sheet retreated giving rise to a reduced elemental leaching and mineral transformations (Hartmann *et al.*, 1999). This contribution thus confirms that the marine depositional environment was absent during the glacial episode in the Southern North Sea (de Gans, 2007). Nowadays, it is generally accepted that composition of ocean-floor clays primarily reflects the continental sediment supply (*e.g.* Biscaye, 1965; Griffin *et al.*, 1968; Petschick *et al.*, 1996). Once settled in sea-water, the continental clay minerals are apparently inert but their exchange capacity is no longer saturated by the same cations (Sayles and Mangelsdorf Jr., 1977). Moreover, the sea-water rich cations like K, Na, and Mg have been shown to be preferentially depleted in waters impregnating the onset of ocean floors (Sayles, 1981) thus presumably giving rise to the neoformation of ordered clay minerals like illite and chlorite by fixation of ions from sea-water (*e.g.* Grim and Johns, 1954). This mechanism is seemingly opposite to the early diagenetic smectitization proposed herein.

The continuity of the fresh water environment beyond the ice-margin in a proglacial lake that covered the whole clinoform succession is furthermore suggested by seismic reflection data (Benvenuti and Moscariello, 2016). Although very little sedimentological and mineralogical evidence for a proglacial lake in the central part of the SNS is provided in the literature, this contribution supports the studies of Gibbard (2007) and Gupta *et al.* (2007) who were first to hypothesize the existence of a large proglacial lake at glacial maximum in the area between the SNS and the Benelux countries. The lacustrine episode in the study area ended with the Holstenian transgression and marine sedimentation that covered the lacustrine deposits on a regional scale, as reported from several occurrences of onshore TVs in the northern part of Germany and The Netherlands (Ehlers and Gibbard, 2004).

The hydromorphic conditions of the glacial period that left traces in clay mineralogy of Unit A (*i.e.* I-S formation, Figure 1) suggest an excess of silica released from dissolved feldspar and quartz (Table 2) that were required for enhanced smectitization (*e.g.* Novikoff *et al.*, 1972). In contrast, in the areas where hydromorphic influences were weaker, or acted for a more restricted time, lesser amounts of

This is a 'pre-publication' version of an accepted article for Clays and Clay Minerals.
This version may be subject to change during the production process.
The DOI given, which may be used for citation purposes, though which will not be active until the version of record is published, is DOI: 10.1346/CCMN.2016.064026

interlayered phases were produced, as shown by lower abundances of I-S in the uppermost part of Unit A, Unit B, and Unit C. The low I-S content of Unit C may, however, be attributed to the return of marine conditions, in line with the more widespread distribution of the deposits of Unit C around the TV boundaries, which coincides with the progressive end of the glacial lacustrine environment at the onset of the Holstenian interglacial (Ehlers and Gibbard, 2004). The presence of I-S in marine pre-glacial deposits, even if in lower percentages than in the TV infill, may still be related to early diagenetic smectitization operating during the glacial stage and facilitated by the large amount of meltwater that percolated into the underlying deposits for hundreds of meters (Kehew *et al.*, 2012 and references therein).

The presence of I-S in sedimentary rocks is traditionally interpreted through the prism of deep-burial diagenesis. Mixed-layer I-S reported from shallower levels of sedimentary sequences (< 1 km) is rarely described in diagenetic studies, mostly due to lack of economic interest. This study offered an alternative approach to the evolution of clay assemblages by studying geologically unique glacial environments, such as tunnel valleys, where the I-S interstratification is linked to early (shallow) diagenesis (smectitization) of detrital illite (and lesser kaolinite). The multimethodological approach used in this study could be applied to clay research of sediment accumulations that are related to Pleistocene glacial events and presently reported extensively in the area of the North Sea, in order to better understand the early‐diagenesis portion of the clay cycle examined in this research.

CONCLUSIONS

(1) Material analyzed from borehole K14-12 located in the K block of Dutch offshore presented a thick succession of Elsterian tunnel valley deposits composed of several units (pre-glacial, A, B, and C) visible on seismic sections.

(2) Grain-size distributions are relatively heterogeneous, with the lower part of succession (lower Unit A) dominated by coarse sand. Higher in the succession, the grain size becomes finer with up to 20 wt% of clay content in the upper portions of Unit A (TV infill), as well as in Units B and C.

This is a 'pre-publication' version of an accepted article for Clays and Clay Minerals.
This version may be subject to change during the production process.
The DOI given, which may be used for citation purposes, though which will not be active until the version of record is published, is DOI: 10.1346/CCMN.2016.064026

(3) Bulk-rock mineralogy of analyzed material is dominated either by quartz or illite, depending on the sediment granulometry. Other phases, notably feldspar and mica, constitute <10 wt%.

(4) XRD and SEM measurements show a clay particle assemblage consisting of illite, mixed-layer illite-smectite, kaolinite and chlorite, with the first and the second being the dominant clay minerals.

(5) Illite is inferred, according to its mineralogical and morphological characteristics (Kübler index, particle size, and shape), to have an unambiguously detrital origin.

(6) The abundances of clay minerals in the stratigraphic succession studied show interlayered I-S enriched in the middle portion of Unit A where illite abundance is lower. I-S abundance was lower in the pre-glacial unit and, especially, in the overlying Units B and C. XRD pattern modelling and deconvolution reveal interlayered I-S to consist of several intermediate phases of different ordering and composition grouped as non-swelling ordered I-S (illite sensu stricto + R3 I-S) and disordered I-S (R0 I-S + R0 I-SS).

(7) The hypothesis of smectitization of illite in a freshwater diagenetic environment is supported by the distribution patterns of I‑S and of the total smectite (Sme_{TOT}), and I-S particle sizes. The smectitization of illite proceeded in a way in which extensive leaching was precluded.

(8) The I-S phase chemistry and speciation of I-S interlayers revealed by modelling of XRD spectra shows that smectitization must have proceeded through a series of mixed-layer I-S intermediates, whereby the illite component was progressively converted to smectite. The chemistry of the I-S octahedral layer suggests that interlayers with maximal Fe content approach I-S compositions with 80 wt% of Sme component, thus corresponding to R0 I-SS as defined by XRD pattern modelling (75-94 wt% Sme). Moreover, the structural formulas of Sme-rich I-S point to the partial allocation of Mg in their interlayer site, which is indicative for restrained chlorite interlayering (~10%) and possible formation of illite-chlorite-smectite clays.

(9) In addition to factors like climate, porosity and permeability, and fluid composition, the grain size of illite particles influences the progress of smectitization as shown by PCA analysis through a

This is a 'pre-publication' version of an accepted article for Clays and Clay Minerals.
This version may be subject to change during the production process.
The DOI given, which may be used for citation purposes, though which will not be active until the version of record is published, is DOI: 10.1346/CCMN.2016.064026

variable load plot where, in addition to the XRD mineralogy, the grain size classes are shown as supplementary variables.

(10) The results of this study are consistent with the hypothesis that formation of mixed-layer I-S by incomplete diagenetic alteration of detrital illite took place in an ice-marginal to proglacial fresh water depositional environment where meltwater must have played a role of degrading fluid responsible for enhanced ion exchange.

ACKNOWLEDGMENT

The present study is the result of a financial support by the GRASP consortium. The Nederlandse Aardolie Maatschappij (Shell) is thanked for providing the sediment material from borehole K14-12. The authors kindly thank P. Gibbard for letting us using his data on the extent of the Pleistocene ice-sheets. F. Gischig is thanked for an outstanding quality of thin and polished sections needed for QEMSCAN®, SEM-EDS, and EMPA investigations. R. Cerny is acknowledged for providing excellent working conditions during extensive XRD measurements. A great appreciation is addressed to S. Carmalt and A. Ristić for their assistance with the English. The authors would also like to thank L. Dominguez and S. Biass as well as the whole Physical volcanology and geological risk research group in Geneva for the use of grain-size analyzer and their help with handling the instrument. Critical comments by A. Süssenberger greatly helped to improve an early version of the manuscript and support of A. Janszen regarding the material provided is greatly appreciated. The manuscript was significantly improved thanks to the review of H. Yalçin. Special thanks to P. Schroeder for editorial handling.

This is a 'pre-publication' version of an accepted article for Clays and Clay Minerals.
This version may be subject to change during the production process.
The DOI given, which may be used for citation purposes, though which will not be active until the version of record is published, is DOI: 10.1346/CCMN.2016.064026

REFERENCES

Adriaens, R. (2015) Neogene and Quaternary clay minerals in the Southern North Sea. PhD thesis, University of Leuven, Belgium, 272 pp.

Aitchinson, J. (1982) The statistical analysis of compositional data. *Journal of the Royal Statistical Society, Series B*, **44**, 139–177.

Allmann, R. (2003) *Röntgen-Pulverdiffraktometrie*. Springer Berlin, Heidelberg, 275 pp.

Bailey, S.W. (1980) Summary of recommendations of AIPEA nomenclature committee on clay minerals. *American Mineralogist*, **65**, 1–7.

Benvenuti, A. and Moscariello, A. (2016) High-resolution seismic geomorphology and stratigraphy of a tunnel valley confined ice-margin fans (Elsterian glaciation, Southern North Sea). *Interpretation-A journal of subsurface characterization*, submitted.

Bijlsma, S. (1981) Fluvial sedimantation from the Fennoscandian area into the north-west European basin during the Late Cenozoic. *Geologie en Mijnbouw/Netherlands Journal of Geosciences*, 337–345.

Biscaye, P.E. (1965) Mineralogy and sedimentation of recent deep- sea clay in the Atlantic Ocean and adjacent seas and oceans. *Geological Society of America Bulletin*, **76**, 803–832.

Blott, S.J. and Pye, K. (2001) GRADISTAT: a grain size distribution and statistics package for the analysis of unconsolidated sediments. *Earth Surface Processes and Landforms*, **26**, 1237–1248.

Boles, J.R. and Franks, S.G. (1979) Clay diagenesis in Wilcox sandstones of Southwest Texas: Implications of smectite diagenesis on sandstone cementation. *Journal of Sedimentary Research*, **49**, 55–70.

Brown, G. and Brindley, G.W. (1980) X-ray diffraction procedures for clay mineral identification. Pp. 305–306 in: *Crystal Structures of Clay Minerals and Their X-Ray Identification*. Mineralogical Society, London.

Chamley, P.D.H. (1989) Terrigenous supply in the ocean. *Springer Berlin Heidelberg*, 163–192.

Cohen, K.M. and Gibbard, P.L. (2010) Global chronostratigraphical correlation table for the last 2.7 million years, v. 2010. *Journal of Quaternary Science*, **2**, 7.

Cuadros, J. and Altaner, S.P. (1998) Characterization of mixed-layer illite-smectite from bentonites using microscopic, chemical, and X-ray methods: Constraints on the smectite-to-illite transformation mechanism. *American Mineralogist*, **83**, 762–774.

Deer, W.A., Howie, R.A., and Zussman, J. (1996) *An introduction to the rock-forming minerals*. 2nd edition. Prentice Hall, Harlow, Essex, England, New York, 712 pp.

Drits, V.A. and Sakharov, B.A. (1976) *X-ray structural analysis of mixed-layer minerals*. Nauka, Moscow.

Dudek, T., Cuadros, J., and Fiore, S. (2006) Interstratified kaolinite-smectite: Nature of the layers and mechanism of smectite kaolinization. *American Mineralogist*, **91**, 159–170.

Eberl, D.D. and Velde, B. (1989) Beyond the Kubler index. *Clay Minerals*, **24**, 571–577.

Ehlers, J. and Gibbard, P.L. (eds.). (2004) *Quaternary glaciations extent and chronology Part I: Europe*. 475 pp.

This is a 'pre-publication' version of an accepted article for Clays and Clay Minerals.
This version may be subject to change during the production process.
The DOI given, which may be used for citation purposes, though which will not be active until the version of record is published, is DOI: 10.1346/CCMN.2016.064026

646 Ferreiro Mählmann, R., Bozkaya, Ö., Potel, S., Bayon, R.L., Šegvić, B., and Nieto, F. (2012) The
647 pioneer work of Bernard Kübler and Martin Frey in very low-grade metamorphic terranes: Paleo-
648 geothermal potential of variation in Kübler-Index/organic matter reflectance correlations. A
649 review. *Swiss Journal of Geosciences*, **105**, 121–152.

650 Folk, R.L. and Ward, W.C. (1957) Brazos River bar [Texas]: A study in the significance of grain size
651 parameters. *Journal of Sedimentary Petrology*, **27**, 3–26.

652 Fordham, A.W. (1990) Weathering of biotite into dioctahedral clay minerals. *Clay Minerals*, **25**, 51–
653 63.

654 de Gans, W. (2007) Quaternary. Pp. 173–195 in: *Geology of the Netherlands* (T.E. Wong, D.A.J.
655 Batjes, and J. de Jager, editors). Royal Netherlands Academy of Arts and Sciences.

656 Gibbard, P.L. (2007) Europe cut adrift. *Nature*, **448**, 259,260.

657 Gottlieb, P., Wilkie, G., Sutherland, D., Ho-Tun, E., Suthers, S., Perera, K., Jenkins, B., Spencer, S.,
658 Butcher, A., and Rayner, J. (2000) Using quantitative electron microscopy for process
659 mineralogy applications. *The Journal of The Minerals, Metals & Materials Society (TMS)*, **52**,
660 24–25.

661 Griffin, J.J., Windom, H., and Goldberg, E.D. (1968) The distribution of clay minerals in the world
662 ocean. *Deep-Sea Research*, **15**, 433–459.

663 Griffioen, J., Klaver, G., and Westerhoff, W.E. (2016) The mineralogy of suspended matter, aquatic
664 and Cenozoic sediments in the Rhine-Meuse-Scheldt delta area, the Netherlands: An overview
665 and review. *Netherlands journal of Geosciences*, 1–85.

666 Grim, R.E. (1968) *Clay Mineralogy*. 2nd edition. McGraw-Hill Book Company, Inc., 596 pp.

667 Grim, R.E. and Johns, W.D. (1954) Clay mineral investigation of sediments in the Northern Gulf of
668 Mexico. *Clays and Clay Minerals*, **327**, 81–103.

669 Guggenheim, S., Bain, D.C., Bergaya, F., Brigatti, M.F., Drits, A., Eberl, D.D., Formoso, M.L.L.,
670 Galan, E., Merriman, R.J., Peacor, D.R., Stanjek, H., and Watanabe, T. (2002) Report of the
671 AIPEA nomenclature committee for 2001: order, disorder and crystallinity in phyllosilicates and
672 the use of the "'Crystallinity Index.'" *Clay Minerals*, **37**, 389–393.

673 Gupta, S., Collier, J.S., Palmer-Felgate, A., and Potter, G. (2007) Catastrophic flooding origin of shelf
674 valley systems in the English Channel. *Nature*, **448**, 342–345.

675 Harding, R. (2015) Evolution of the giant southern North Sea shelf prism: Testing Sequence
676 stratigraphic concepts and the global sea level curve with full three dimensional control. PhD
677 thesis, University of Manchester, UK.

678 Hartmann, B.H., Juhász Bodnár, K., Ramseyer, K., and Matter, A. (1999) Effect of Permo-
679 Carboniferous climate on illite-smectite, Haushi Group, Sultanate of Oman. *Clays and Clay*
680 *Minerals*, **47**, 131–143.

681 Hey, M. (1954) A new review of the chlorites. *Mineralogical Magazine*, **30**, 277–292.

682 Hong, H., Churchman, G.J., Gu, Y., Yin, K., and Wang, C. (2012) Kaolinite–smectite mixed-layer
683 clays in the Jiujiang red soils and their climate significance. *Geoderma*, **173-174**, 75–83.

684 Huggett, J.M. and Knox, R.W.O. (2006) Clay mineralogy of the Tertiary onshore and offshore strata
685 of the British Isles. *Clay Minerals*, **41**, 5–46.

686 Huuse, M. and Lykke-Andersen, H. (2000) Overdeepened Quaternary valleys in the eastern Danish

This is a 'pre-publication' version of an accepted article for Clays and Clay Minerals.
This version may be subject to change during the production process.
The DOI given, which may be used for citation purposes, though which will not be active until the version of record is published, is DOI: 10.1346/CCMN.2016.064026

North Sea: Morphology and origin. *Quaternary Science Reviews*, **19**, 1233–1253.

Iacoviello, F., Giorgetti, G., Nieto, F., and Memmi, I. (2012) Evolution with depth from detrital to authigenic smectites in sediments from AND-2A drill core (McMurdo Sound, Antarctica). *Clay Minerals*, **47**, 481–498.

Irion, G. and Zöllmer, V. (1999) Clay mineral associations in fine-grained surface sediments of the North Sea. *Journal of Sea Research*, **41**, 119–128.

Jackson, M.L. (1957) Frequency distribution of clay minerals in major great soil groups as related to the factors of soil formation. *Clays and Clay Minerals*, **6**, 133–143.

Kehew, A.E., Piotrowski, J.A., and Jørgensen, F. (2012) Tunnel valleys: Concepts and controversies — A review. *Earth-Science Reviews*, **113**, 33–58. Elsevier B.V.

Kemp, S.J. and Merriman, R.J. (2009) Polyphase low-grade metamorphism of the Ingleton Group, northern England, UK: A case study of metamorphic inversion in a mudrock succession. *Geological Magazine*, **146**, 237–251.

Kretz, R. (1983) Symbols for rock-forming minerals. *American Mineralogist*, **68**, 277–279.

Kübler, B. (1964) Les argiles, indicateurs de métamorphisme. *Revue de l'Institut Français du Pétrole*, **19**, 1093–1112.

Kuhlmann, G., de Boer, P.L., Pedersen, R.B., and Wong, T.E. (2004) Provenance of Pliocene sediments and paleoenvironmental changes in the southern North Sea region using Samarium–Neodymium (Sm/Nd) provenance ages and clay mineralogy. *Sedimentary Geology*, **171**, 205–226.

Laban, C. (1995) The Pleistocene glaciations in the Dutch sector of the North Sea. PhD thesis, University of Amsterdam.

Lagaly, G., Ogawa, M., and Dékány, I. (2006) Clay mineral organic interactions. Pp. 309–377 in: *Developments in Clay Science* (F. Bergaya, B.K.G. Theng, and G. Lagaly, editors). Handbook of Clay Science, Elsevier.

Lanson, B. (1993) *DECOMPXR, X-ray diffraction pattern decomposition program*. ERM, Poitiers, France, 48 pp.

Lanson, B. and Besson, G. (1992) Characterization of the end of smectite-to-llite transformation: Decomposition of X-ray patterns. *Clays and Clay Minerals*, **40**, 40–52.

Lanson, B. and Velde, B. (1992) Decomposition of X-ray diffraction patterns: A convenient way to describe complex I-S diagenetic evolution. *Clays and Clay Minerals*, **40**, 629–643.

Lê, S., Josse, J., and Husson, F. (2008) FactoMineR: An R package for multivariate analysis. *Journal of Statistical Software*, **25**, 1–18.

Lee, J.R., Busschers, F.S., and Sejrup, H.P. (2012) Pre-Weichselian Quaternary glaciations of the British Isles, The Netherlands, Norway and adjacent marine areas south of 68N. implications for long-term ice sheet. *Quaternary Science Reviews*, **44**, 213–228.

Leipe, T. and Sea, B. (2003) The kaolinite/chlorite clay mineral ratio in surface sediments of the southern Baltic Sea as an indicator for long distance transport of fine-grained material. *Baltica*, **16**, 31–36.

de Lugt, I. (2007) Stratigraphical and structural setting of the Palaeogene siliciclastic sediments in the Dutch part of the North Sea Basin. PhD thesis, University of Utrecht, 112 pp.

This is a 'pre-publication' version of an accepted article for Clays and Clay Minerals.
This version may be subject to change during the production process.
The DOI given, which may be used for citation purposes, though which will not be active until the version of record is published, is DOI: 10.1346/CCMN.2016.064026

728 Mangerud, J. and Jansen, E. (1996) Late cCenozoic history of the Scandinavian and Barents Sea ice
729 sheets. *Global and Plaretary Change*, **12**, 11–26.

730 Meunier, A. (2007) Soil hydroxy-interlayered minerals: A re-interpretation of their crystallochemical
731 properties. *Clays and Clay Minerals*, **55**, 380–388.

732 Meunier, A. and Velde, B.D. (2004) *Illite - origins, evolution and metamorphism*. Springer Verlag,
733 288 pp.

734 Millot, G. (1971) *Geology of clays. Weathering, sedimentology, geochemistry*. Springer-Verlag, 429
735 pp.

736 Moore, D.M. and Reynolds, J. (1997) *X-Ray diffraction and the identification and analysis of clay*
737 *minerals*. Oxford University Press, 378 pp.

738 Moreau, J., Huuse, M., Janszen, A., van der Vegt, P., Gibbard, P.L., and Moscariello, A. (2012) The
739 glaciogenic unconformity of the southern North Sea. *Geological Society, London, Special*
740 *Publications*, **368**, 99–110.

741 Murton, D.K. and Murton, J.B. (2012) Middle and Late Pleistocene glacial lakes of lowland Britain
742 and the southern North Sea Basin. *Quaternary International*, **260**, 115–142. Elsevier Ltd and
743 INQUA.

744 Nielsen, O.L.E.B., Rasmussen, E.S., and Thyberg, B.I. (2015) Distribution of clay minerals in the
745 Northern North Sea Basin during the Paleogene and Neogene: A result of source-area geology
746 and sorting processes. *Journal of Sedimentary Research*, **85**, 562–581.

747 Norrish, K. and Pickering, J.G. (1983) Clay minerals. Pp. 281–308 in: *Soils, an Australian Viewpoint*.
748 Division of Soils, CSIRO, Academic Press, London.

749 Novikoff, A., Tsawlassou, U., Gac, J.Y., Bourgeat, F., and Tardy, Y. (1972) Altération des biotites
750 dans les arènes des pays tempérés, tropicaux et équatoriaux. *Sciences Géologiques. Bulletin*, **25**,
751 287–305.

752 Petschick, R., Kuhn, G., and Gingele, F. (1996) Clay mineral distribution in surface sediments of the
753 South Atlantic: sources, transport, and relation to oceanography. *International Journal of Marine*
754 *Geology, Geochemistry and Geophysics*, **130**, 203–229.

755 Pouchou, J.L. and Pichoir, F. (1984) A new model for quantitative analyses. I. Application to the
756 analysis of homogeneous samples. *La Recherche Aérospatiale*, **3**, 13–38.

757 Pouchou, J.L. and Pichoir, F. (1985) "PAP" ($\varphi-\rho-Z$) correction procedure for improved quantitative
758 microanalysis. Pp. 104–106 in: *Microbeam Analysis* (J.T. Armstrong, editor). San Francisco
759 Press, San Francisco.

760 Praeg, D. (1996) Morphology, stratigraphy and genesis of buried Mid-Pleistocene tunnel-valleys in the
761 Southern North Sea Basin. PhD thesis, University of Edinburgh, 207 pp.

762 Ramseyer, K. and Boles, J.R. (1986) Mixed-layer illite/smectite minerals in Tertiary sandstones and
763 shales, San Joaquin Basin, California. *Clays and Clay Minerals*, **34**, 115–124.

764 Reynolds, R.C. and Hower, J. (1970) The nature of interlayering in mixed-layer illite-
765 montmorillonites. *Clays and Clay Minerals*, **18**, 25–36.

766 Rieder, M., Cavazzini, G., D'yakonov, Y.S., Frank-Kamenetskii, V.A., Gottardi, G., Guggenheim, S.,
767 Koval', P.V., Mueller, G., Neiva, A.M.R., Radoslovich, E.W., Robert, J.-L., Sassi, F.P., Takeda,
768 H., Weiss, Z., and Wones, D.R. (1998) Nomenclature of the micas. *The Canadian Mineralogist*,
769 **36**, 905–912.

This is a 'pre-publication' version of an accepted article for Clays and Clay Minerals.
This version may be subject to change during the production process.
The DOI given, which may be used for citation purposes, though which will not be active until the version of record is published, is DOI: 10.1346/CCMN.2016.064026

Sayles, F.L. (1981) The composition and diagenesis of interstitial solutions—II. Fluxes and diagenesis at the water-sediment interface in the high latitude North and South Atlantic. *Geochimica et Cosmochimica Acta*, **45**, 1061–1086.

Sayles, F.L. and Mangelsdorf Jr., P.C. (1977) The equilibration of clay minerals with sea water: exchange reactions. *Geochimica et Cosmochimica Acta*, **41**, 951–960.

Schaetzl, R. and Thompson, M.L. (2015) *Soils: Genesis and Geomorphology*. 2nd edition. Cambridge University Press, 795 pp.

Schultz, L.G., Shepard, A.O., Blackmon, P.D., and Starkey, H.C. (1971) Mixed–layer kaolinite-montmorillonite from the Yucatan Peninsula, Mexico. *Clays and Clay Minerals*, **19**, 137–150.

Sengupta, P., Saikia, P.C., and Borthakur, P.C. (2008) SEM-EDX characterization of an iron-rich kaolinite clay. *Journal of Scientific and Industrial Research*, **67**, 812–818.

Shell (1993) *K14-12 end of well report: NLOG_GS_PUB_9409_IG8098006_K14-12*. 10 pp.

Smoot, T.W. (1960) *Clay mineralogy of pre-Pennsylvanian sandstones and shales of the Illinois Basin, Part-I. Relation of permeability to clay mineral suite*. Illinois state geological survey, 20 pp.

Środoń, J. (2006) Identification and quantitative analysis of clay minerals. Pp. 767–787 in: *Developments in Clay Science* (F. Bergaya, B.K.G. Theng, and G. Lagaly, editors). Handbook of Clay Science, Elsevier.

Thorez, J. (1989) Between the crystal and the solutions. A graphical overview of the passage to, from and of the clay minerals in the lithosphere during weathering. Pp. 49–120 in: *Weathering; Its Products and Deposits. Processes* (V.P. Evangelou, G. Faure, J. Goni, P.L.C. Grubb, P.A. Hill, O. Lahondney-Sarc, A.J. Melfi, E. Mendelovici, A.P. Nikitina, W.F. Pickering, and S.S. Augustithis, editors). Theophrastus Publishers S. A., Greece.

Uzarowicz, Ł., Šegvić, B., Michalik, M., and Bylina, P. (2012) The effect of hydrochemical conditions and pH of the environment on phyllosilicate transformations in the weathering zone of pyrite-bearing schists in Wieściszowice (SW Poland). *Clay Minerals*, **47**, 401–417.

van der Vegt, P., Janszen, A., and Moscariello, A. (2012) Tunnel valleys: Current knowledge and future perspectives. *Geological Society, London, Special Publications*, **368**, 75–97.

Velde, B. (1985) *Clay minerals: A physico-chemical explanation of their occurrence*. in: *Developments in Sedimentology*. Elsevier, Amsterdam, New York, 427 pp.

Warr, L.N. and Rice, A.H.N. (1994) Interlaboratory standardization and calibration of clay mineral crystallinity and crystallite size data. *Journal of Metamorphic Geology*, **12**, 141–152.

Weaver, C.E. and Beck, K.C. (1971) Clay-Water Diagenesis During Burial or How Mud Becomes Gneiss. *Geological Society of America Special Papers*, **134**, 1–78.

Welton, J.E. (1984) *SEM Petrology Atlas*. The American Association of Petroleum Geologists. Methods in Exploration Series, 4, Tulsa, Oklahoma, U.S.A.

Westerhoff, W. (2009) Stratigraphy and sedimentary evolution: The lower Rhine-Meuse system during the Late Pliocene and Early Pleistocene (southern North Sea Basin). PhD thesis, University of Amsterdam.

Whitney, D.L. and Evans, B.W. (2010) Abbreviations for names of rock-forming minerals. *American Mineralogist*, **95**, 185–187.

This is a 'pre-publication' version of an accepted article for Clays and Clay Minerals.
This version may be subject to change during the production process.
The DOI given, which may be used for citation purposes, though which will not be active until the version of record is published, is DOI: 10.1346/CCMN.2016.064026

811 Whittig, L.D. and Jackson, M.L. (1955) Mineral content and distribution as indexes of weathering in
812 the Omega and Ahmeek soils of Northern Wisconsin. *Clays and Clay Minerals*, **4**, 362–371.

813 Zagwijn, W.H. (1989) The Netherlands during the Tertiary and the Quaternary: A case history of
814 coastal lowland evolution. *Geologie en Mijnbouw*, **68**, 107–120.

815 Zuther, M., Brockamp, O., and Clauer, N. (2000) Composition and origin of clay minerals in
816 Holocene sediments from the south-eastern North Sea. *Sedimentology*, **47**, 119–134.

817

818

This is a 'pre-publication' version of an accepted article for Clays and Clay Minerals.
This version may be subject to change during the production process.
The DOI given, which may be used for citation purposes, though which will not be active until the version of record is published, is DOI: 10.1346/CCMN.2016.064026

FIGURE CAPTIONS

Figure 1. Map shows a schematic representation of the drainage system of the Southern North Sea at Early Pleistocene and the most important features regarding the successive glaciations (*i.e.* ice-sheet margins and tunnel valleys). The location of the study area is marked in white. Main river systems are after de Gans (2007) and Westerhoff (2009) indicating the source areas of detrital material. Continuous lines in yellow, blue, and red mark the positions of ice-margins at glacial maxima and are reproduced with the permission of the author, Philip Gibbard, from *www.qpg.geog.cam.ac.uk/research/projects/nweurorivers/*. The numerous tiny black lines and the red line in the study area indicate the large number of glacial incisions created during repeated glaciations in NW Europe and are redrawn after van der Vegt *et al.* (2012). The proglacial lacustrine environment created at the Elsterian glacial maximum is modified after Murton and Murton (2012).

Figure 2. (a) Map shows the depths (expressed in two way time) of the glacial unconformity mapped on 3D high resolution seismic data by Moreau *et al.* (2012). A large number of incisions (tunnel valleys) are evident in this reconstruction. The location of the seismic reflection profile is indicated by a black line and the black dot shows the location of borehole K14-12, (b) N-S oriented seismic section showing the stratigraphic architecture. The tunnel valley base is highlighted in red, separating the pre-glacial deposits from the overlying TV infill. The main infill of the tunnel valley is defined by a thick interval of northward dipping reflectors (Unit A), overlain by a thin interval of horizontal reflectors in a restricted area (Unit B), and a widespread interval characterized by a chaotic seismic facies (Unit C). Well K14-12 is identified by a red vertical line. A constant velocity of 1900 m/s was used for time-depth conversion (Benvenuti and Moscariello, 2016), (c) a histogram showing the grain size distributions with the green line showing mean values (Folk and Ward, 1957) for 36 sediment samples (from ditch cuttings). The illite/quartz ratio was calculated from QEMSCAN® data. The stratigraphic succession of the TV infill and post-glacial deposits is modified after Benvenuti and Moscariello (2016).

This is a 'pre-publication' version of an accepted article for Clays and Clay Minerals.
This version may be subject to change during the production process.
The DOI given, which may be used for citation purposes, though which will not be active until the version of record is published, is DOI: 10.1346/CCMN.2016.064026

Figure 3. Mineral composition of analyzed clay factions (< 0.2 μm) shown for three representative samples. EG stands for the treatment with ethylene-glycol and AD for air-dried samples. Measurements after heating are not shown (see text). Mineral symbols: I-S (illite-smectite), Chl (chlorite), Ill (illite), and Kln (kaolinite).

Figure 4. Comparison between experimental (zigzag line) and calculated (continuous line) XRD patterns for three representative measurements on clay fractions (air-dried).

Figure 5. Decomposition of XRD patterns of the clay fraction (air-dried) for three representative samples. The experimental XRD patterns are zigzag and black, the best fits are continuous and red, while elementary Gaussian curves are continuous and light grey.

Figure 6. SEM imagery of different sediment samples showing (a) illite and I-S crystals forming irregular flake-like platelets oriented parallel to each other, (b) rod-like illite and relatively coarse chlorite and kaolinite agglomerates, (c) agglomerates of smectite-rich interlayered I-S, and (d) chlorite mineralization growing at the expenses of biotite. The points and digits placed on some of the minerals stand for microprobe analyses and their corresponding numbers. The representative microprobe data are provided in **Table 4**.

Figure 7. (a) The variable projection image illustrating the correlation of smectite-rich phases with the finest grain fraction, and conversely the association of chlorite and illite with the coarsest grain fraction, (b) the principal component biplot (Dim 1 and Dim2) based on the fine fraction mineralogical composition and grain-size classes, showing samples grouping according to their stratigraphical position.

Figure 8. Mineral differentiation diagrams based on the phase chemistry of micas, illite, and interstratified I-S. (a) Ca-K-Mg ternary diagram showing a trend of Ca and Mg enrichment in the illite and I-S, (b) $Al^{IV} – Al^{VI} + Fe^{3+} – Mg$ ternary diagram illustrates the changes in octahedral composition

This is a 'pre-publication' version of an accepted article for Clays and Clay Minerals.
This version may be subject to change during the production process.
The DOI given, which may be used for citation purposes, though which will not be active until the version of record is published, is DOI: 10.1346/CCMN.2016.064026

reflecting a smectitization process, (c) K – Si/Al plot depicts the relationship of interlayer K net loss with Al-Si replacement during smectitization. For details, see the text.

This is a 'pre-publication' version of an accepted article for Clays and Clay Minerals.
This version may be subject to change during the production process.
The DOI given, which may be used for citation purposes, though which will not be active until the version of record is published, is DOI: 10.1346/CCMN.2016.064026

Table 1. Sybilla© modelling parameters of mixed-layer phases (R0 I-S, R0 I-SS, R3 I-S, and R0 K-S)

Samples/ Phase parameters	220	240	310	350	370	440	530
σ* (R0 I-S)	12	12	12	12	11	11	11
CSDS (R0 I-S)	7	7	7	7	7	7	7
Sme (R0 I-S)	20	20	26	31	28	28	21
σ* (R0 I-SS)	12	12	12	12	12	12	12
CSDS (R0 I-SS)	5	5	5	5	5	5	5
Sme (R0 I-SS)	81	81	81	92	94	82	75
σ* (R3 I-S)	12	12	12	12	12	12	12
CSDS (R3 I-S)	12	15	15	15	15	15	15
Sme (R3 I-S)	5	5	5	5	9	9	13
σ* (R0 K-S)	10	10	10	10	10	10	10
CSDS (R0 K-S)	7	7	7	7	7	7	7
Sme (R0 K-S)	2	2	2	2	6	6	1

σ* - orientation of particles on the mounted X-ray slide; CSDS - coherent scattering domain sizes expressed in layers; Sme – smectite content in the respective mixed-layer mineral (in wt%); I-S and K-S – mixed-layer illite-smectite and kaolinite-smectite, respectively; R – Reichweit (measure of order); Parameters of R0 I-SSS not given as this entry is used to mimic I-S superstructure 001^{*} diffraction peak partly masked by primary radiation.

This is a 'pre-publication' version of an accepted article for Clays and Clay Minerals.
This version may be subject to change during the production process.
The DOI given, which may be used for citation purposes, though which will not be active until the version of record is published, is DOI: 10.1346/CCMN.2016.064026

Table 2. Modal mineralogy based on QEMSCAN and XRD whole-rock measurements

Sample	*Qtz*	*Pl*	*Kfs*	*Cal/Arg*	*Dol*	*Ms*	*Bt*	*Ill*	*Sme*	*Kln*	*Chl*	*Sd*	*Py*	*HMs*	*Unclass.*	*I/Qtz*
200	21.18	3.64	1.35	3.98	1.18	1.67	4.09	55.47	0.32	1.08	1.90	0.26	0.63	0.34	2.90	2.62
210	21.68	3.54	1.58	3.63	1.14	1.60	5.13	56.04	0.27	0.95	2.00	0.08	0.53	0.39	1.44	2.58
220	12.13	2.37	0.74	3.80	0.44	1.65	6.16	60.56	0.21	1.02	2.15	0.11	5.17	0.24	3.24	4.99
230	15.53	2.76	1.24	0.92	0.36	1.08	10.71	58.80	0.77	0.82	4.13	0.02	0.78	0.25	1.83	3.78
240	30.13	5.06	3.27	2.82	1.27	1.34	2.21	47.66	0.14	0.85	1.02	0.09	0.87	0.41	2.86	1.58
250	19.40	3.69	1.94	1.53	0.63	0.88	3.59	63.01	0.20	0.67	1.73	0.04	0.62	0.30	1.78	3.24
260	31.54	3.76	2.70	1.28	0.64	0.81	4.80	49.71	0.16	0.59	1.43	0.02	0.70	0.38	1.46	1.57
270	29.59	4.71	2.46	1.71	0.81	1.16	4.88	48.45	0.30	0.80	2.21	0.05	0.89	0.46	1.53	1.63
280	17.19	2.66	1.45	0.96	0.36	0.91	6.92	64.13	0.26	0.68	2.06	0.02	0.90	0.21	1.31	3.73
290	28.05	3.51	2.34	1.61	0.68	1.10	4.50	52.85	0.25	0.83	2.20	0.06	0.69	0.35	0.97	1.88
300	25.98	3.52	1.81	1.48	0.48	0.87	5.94	55.33	0.17	0.54	1.22	0.04	0.69	0.29	1.64	2.13
310	36.99	3.01	2.63	1.72	0.68	0.90	2.49	45.46	0.09	0.60	0.68	0.59	0.75	0.26	3.14	1.23
320	37.40	3.99	2.78	1.85	0.64	0.89	3.19	42.79	0.14	0.49	0.97	0.05	0.81	0.26	3.74	1.14
330	45.52	3.83	3.39	2.19	0.56	0.57	1.38	37.97	0.09	0.40	0.82	0.03	0.77	0.29	2.18	0.83
340	34.97	3.29	2.78	1.35	0.53	0.70	1.98	49.15	0.17	0.62	1.57	0.07	0.54	0.25	2.03	1.40
350	42.76	3.73	3.54	1.51	0.61	0.72	2.07	41.03	0.11	0.49	0.91	0.05	0.64	0.31	1.52	0.96
360	44.18	4.50	3.59	1.72	0.69	0.82	1.64	38.38	0.12	0.49	1.11	0.07	1.16	0.43	1.13	0.86
370	48.31	4.19	3.64	1.51	0.54	0.69	1.52	33.82	0.11	0.46	0.99	0.06	1.87	0.34	1.94	0.70
380	44.74	4.07	3.72	6.49	0.51	0.73	1.57	28.33	0.09	0.40	0.70	0.05	6.09	0.34	2.16	0.63
390	47.38	3.56	3.10	8.24	0.48	0.55	1.21	24.25	0.08	0.32	0.46	0.05	8.69	0.30	1.33	0.51
400	48.41	3.68	3.59	9.92	0.53	0.54	0.93	28.06	0.08	0.40	0.75	0.52	0.86	0.33	1.41	0.58
410	48.79	4.64	3.26	7.25	0.50	0.72	1.99	28.11	0.14	0.36	0.61	0.23	1.16	0.32	1.92	0.57
420	47.00	3.07	3.38	9.51	0.39	0.54	1.74	26.80	0.11	0.37	0.55	0.04	1.74	2.91	1.84	0.57
430	60.82	3.12	3.41	11.83	0.38	0.47	0.77	16.68	0.08	0.21	0.34	0.02	0.76	0.24	0.88	0.27
440	35.93	2.81	2.12	7.98	0.48	0.78	3.18	41.78	0.23	0.47	1.67	0.05	1.22	0.25	1.02	1.16
450	52.37	2.11	1.98	20.36	0.30	0.32	0.63	14.91	0.08	0.20	0.28	0.02	3.91	0.20	2.34	0.28
460	55.29	1.78	2.11	26.27	0.25	0.35	0.37	7.73	0.03	0.22	0.38	0.11	4.28	0.28	0.54	0.14
470	42.30	2.21	5.04	43.35	0.11	0.14	0.19	3.82	0.02	0.09	0.19	0.02	0.62	0.16	1.76	0.09
480	64.10	1.54	1.36	27.14	0.20	0.21	0.17	2.69	0.03	0.13	0.18	0.02	1.00	0.20	1.02	0.04
490	60.16	3.95	7.20	19.12	0.57	0.35	0.34	5.24	0.03	0.15	0.45	0.03	0.94	0.36	1.10	0.08
500	26.35	1.77	1.03	14.74	0.28	0.49	2.90	48.92	0.14	0.51	1.00	0.08	0.77	0.16	0.84	1.85
510	27.14	1.76	5.14	23.29	0.31	0.43	0.90	32.54	0.06	0.67	0.52	2.01	2.47	0.13	2.63	1.20
520	17.77	1.68	1.02	12.59	0.87	0.49	0.53	53.01	0.20	2.08	0.66	0.06	3.47	0.16	5.39	2.98
530	15.07	1.33	0.83	4.97	0.17	0.60	3.41	55.79	0.14	0.82	0.97	2.28	8.67	0.13	4.83	3.70
540	23.57	1.47	1.35	21.27	1.78	0.57	2.04	41.40	0.20	0.85	0.98	0.05	1.55	0.62	2.31	1.75
550	15.18	1.25	0.57	20.54	1.03	0.53	2.05	45.25	0.17	0.88	1.01	0.04	6.96	0.14	4.39	2.98

Components are expressed in wt%. Qtz: quartz; Pl: plagioclase; Kfs: K-feldspar; Cal/Arg: calcite/aragonite; Dol: dolomite; Ms: muscovite; Bt: biotite; Ill: illite; Sm: smectite; Kln: kaolinite; Chl: chlorite; Sd: siderite; Py: pyrite; HMs: transparent heavy minerals (hornblende, epidote, garnet); Unclass.: QEMSCAN unclassified data. Mineral abbreviations after Kretz (1983) and Whitney and Evans (2010).

This is a 'pre-publication' version of an accepted article for Clays and Clay Minerals.
This version may be subject to change during the production process.
The DOI given, which may be used for citation purposes, though which will not be active until the version of record is published, is DOI: 10.1346/CCMN.2016.064026

Table 3. Relative clay mineral abundances in analyzed samples (in wt%)

Sample	Ill (s.s.)	Kln	Chl	R3 I-S	R0 I-S	R0 I-SS	R0 I-SSS	R0 K-S	Sme_{TOT}
220	18	8	8	34	20	3	2	7	8
240	23	8	7	18	23	2	4	15	11
310	15	7	5	19	35	4	4	11	16
350	14	9	5	22	29	3	8	10	20
370	17	9	6	17	29	3	6	13	18
440	19	10	5	19	25	7	5	10	17
530	13	10	5	26	20	4	2	20	12

I-S and K-S – mixed-layer illite-smectite and kaolinite-smectite, respectively; R – Reichweit (measure of order); Sme_{TOT} – total smectite content in all I-S mixed-layer phases containing smectite, only R0 I-SSS not considered; Ill (s.s.): illite sensu stricto; Kln: kaolinite; Chl-chlorite. Mineral abbreviations after Kretz (1983) and Whitney and Evans (2010).

This is a 'pre-publication' version of an accepted article for Clays and Clay Minerals.
This version may be subject to change during the production process.
The DOI given, which may be used for citation purposes, though which will not be active until the version of record is published, is DOI: 10.1346/CCMN.2016.064026

Table 4. Selected microprobe analyses and formulae of illite, chlorite, illite-smectite, muscovite, and biotite

	illite				*illite/smectite*								kaolinite		*chlorite*	muscovite		*biotite*	
Sample	240	410	310	220	*240*	*370*	*350*	*530*	*310*	*240*	*410*	*530*	310	530	*310*	240	410	*310*	*220*
Anal. No.	3	8	5	2	6	2	12	2	13	15	12	5	12	13	2	1	10	4	7
SiO_2	48.63	47.79	46.63	47.49	44.97	45.53	39.72	41.28	38.31	45.30	39.22	41.12	42.41	45.35	26.80	47.29	48.39	48.17	45.14
TiO_2	0.29	0.77	0.21	0.45	0.64	0.36	0.23	0.65	1.13	0.17	0.51	0.36	0.02	0.07	0.07	0.51	0.56	2.34	1.85
Al_2O_3	30.63	21.62	27.45	25.32	20.59	22.74	20.59	19.05	17.05	30.01	17.14	19.04	34.00	29.69	21.82	36.49	32.61	19.85	21.09
Fe_2O_3																			
FeO	2.89	6.82	3.10	4.24	5.74	5.39	7.56	5.75	8.4	2.00	5.00	5.34	3.82	2.66	25.10	1.01	2.56	11.16	14.63
MnO	0.02	0.07	0.05	0.03	0.04	0.03	0.08	0.04	0.15	0.03	0.04	0.05	0.01	0.00	0.25	0.01	0.02	0.13	0.14
MgO	1.62	3.31	2.07	2.43	2.49	2.56	3.73	2.77	4.05	1.14	2.16	2.54	0.67	0.98	13.69	0.75	1.03	6.83	5.46
CaO	0.40	0.58	0.42	0.41	0.64	0.50	1.17	0.72	1.12	1.05	1.78	2.26	0.10	0.16	0.04	0.03	0.53	0.35	0.89
Na_2O	0.43	1.21	0.71	1.04	0.90	1.37	1.02	0.90	0.64	0.25	0.99	0.85	0.49	0.09	1.70	0.82	0.89	0.47	0.00
K_2O	2.82	4.88	6.59	5.62	3.33	4.43	3.83	3.25	3.22	2.28	3.18	2.30	0.15	2.15	0.12	8.09	8.60	5.64	6.31
Total	87.05	87.23	87.03	79.34	79.34	82.92	77.93	74.41	74.08	82.23	70.01	73.86	81.51	81.57	87.97	95.85	95.12	95.35	95.97
Si	3.332	3.427	3.321	3.383	3.485	3.405	3.213	3.432	3.265	3.301	3.481	3.435	2.834	3.043	2.798	3.084	3.210	3.324	3.178
Al^{IV}	0.668	0.573	0.679	0.617	0.515	0.595	0.787	0.568	0.735	0.699	0.519	0.565	1.166	0.957	1.202	0.916	0.790	0.676	0.822
TC	0.668	0.573	0.679	0.617	0.515	0.595	0.787	0.568	0.735	0.699	0.519	0.565	1.166	0.957	1.202	0.916	0.790	0.676	0.822
Ti	0.015	0.041	0.011	0.024	0.037	0.020	0.014	0.040	0.073	0.010	0.034	0.023	0.001	0.004	0.005	0.025	0.028	0.122	0.098
Al^{VI}	1.805	1.254	1.625	1.509	1.366	1.409	1.176	1.299	0.978	1.878	1.274	1.309	1.511	1.391	1.483	1.889	1.759	0.938	0.928
Fe^{3+}	0.166	0.409	0.184	0.253	0.372	0.337	0.511	0.400	0.599	0.122	0.371	0.373							
Fe^{2+}													0.214	0.149	2.191	0.055	0.142	0.644	0.861
Mn	0.001	0.005	0.003	0.002	0.003	0.002	0.005	0.003	0.011	0.002	0.003	0.004	0.000	0.000	0.022	0.001	0.001	0.007	0.008
Mg	0.165	0.353	0.219	0.258	0.288	0.285	0.436	0.343	0.477	0.124	0.286	0.316	0.066	0.098	2.131	0.060	0.102	0.698	0.543
TOC	1.999	2.062	2.042	2.046	2.066	2.053	2.142	2.085	2.138	2.136	1.968	2.025	1.792	1.642	5.832	2.030	2.032	2.409	2.438
OC		0.131	0.085	0.098	0.056	0.108	0.001	0.051	0.001		0.351	0.222		1.317		0.001	0.121	0.000	0.000
Mg							0.014		0.038							0.013		0.005	0.030
Ca	0.029	0.045	0.032	0.032	0.053	0.040	0.102	0.064	0.102	0.082	0.169	0.202	0.007	0.011	0.004	0.002	0.038	0.026	0.067
Na	0.057	0.168	0.098	0.144	0.135	0.199	0.159	0.145	0.106	0.035	0.170	0.137	0.044	0.064	0.019	0.214	0.105	0.119	0.064
K	0.247	0.446	0.599	0.511	0.329	0.423	0.395	0.345	0.350	0.212	0.360	0.245	0.013	0.184	0.016	0.673	0.728	0.496	0.567
ILC		0.704	0.761	0.719	0.570	0.702	0.786	0.618	0.736		0.868	0.786		0.270		0.917	0.909	0.677	0.825
TLC		0.704	0.764	0.715	0.571	0.703	0.788	0.619	0.736		0.870	0.787		2.274		0.917	0.911	0.676	0.822
OH-	2	2	2	2	2	2	2	2	2	2	2	2	8	8	8	2	2	2	2
Total	6.486	6.721	6.772	6.731	6.583	6.715	6.813	6.639	6.734	6.463	6.667	6.61	5.856	5.901	9.871	6.932	6.903	7.055	7.165

Chlorite is calculated on the basis of 14 oxygens / 8(OH) and all Fe as FeO. Kaolinite is calculated on the basis of 7 oxygens / 4(OH). Mica and illite are calculated on basis of 11 oxygens / 2(OH) and all Fe as FeO and Fe_2O_3, respectively. Illite/smectite is calculated on basis of 11 oxygens / 2(OH), all Fe as Fe_2O_3, and no interlayer water. TC=Tetrahedral Charge, TOC=Total Octahedral Cation, OC=Octahedral Charge, ILC=Interlayer Charge, TLC=Total Layer Charge

This is a 'pre-publication' version of an accepted article for Clays and Clay Minerals.
This version may be subject to change during the production process.
The DOI given, which may be used for citation purposes, though which will not be active until the version of record is published, is DOI: 10.1346/CCMN.2016.064026

Figure 1

Click here to download Figure Figure 1.tif

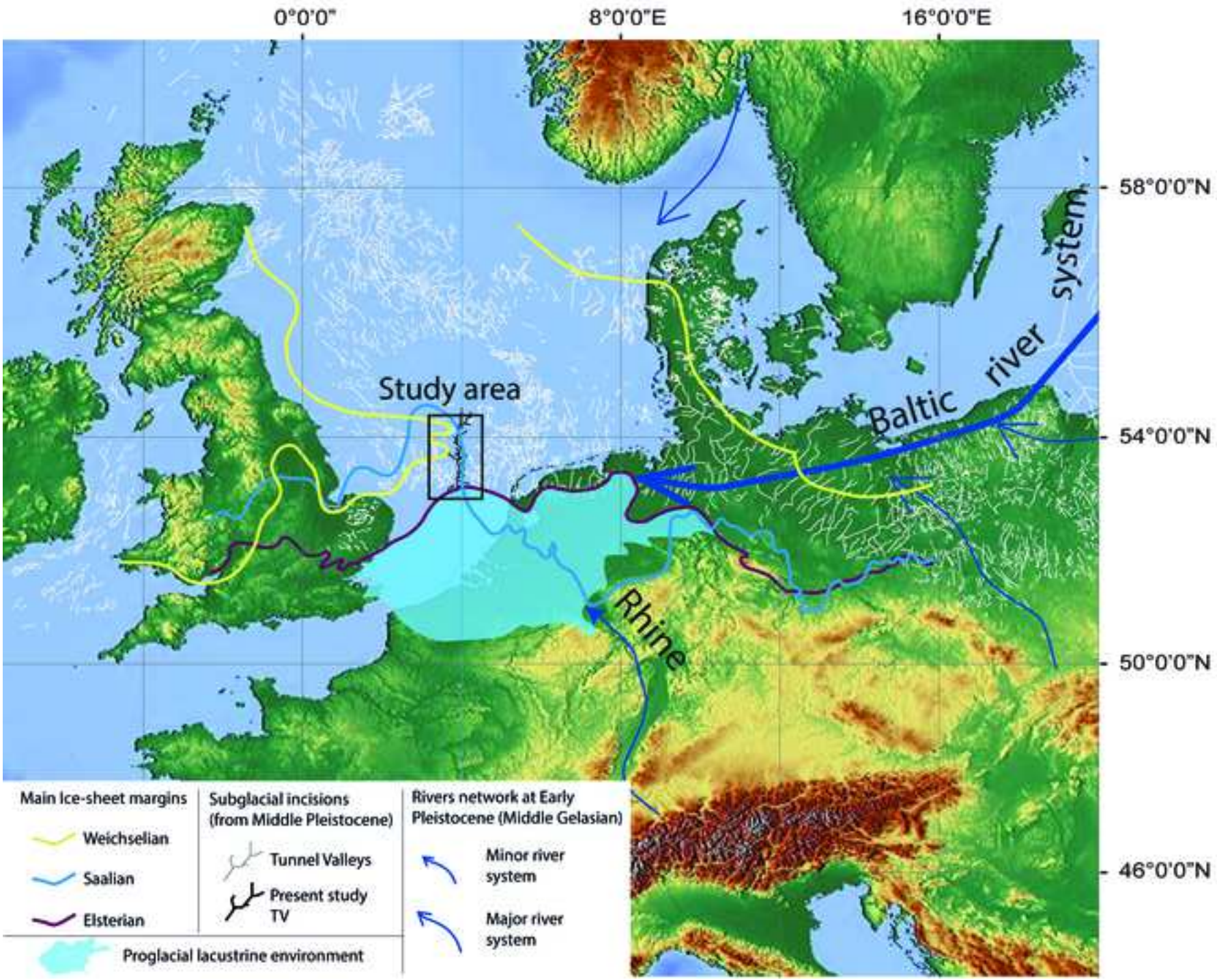

This is a 'pre-publication' version of an accepted article for Clays and Clay Minerals.
This version may be subject to change during the production process.
The DOI given, which may be used for citation purposes, though which will not be active until the version of record is published, is DOI: 10.1346/CCMN.2016.064026

Figure 2

Click here to download Figure Figure 2.tif

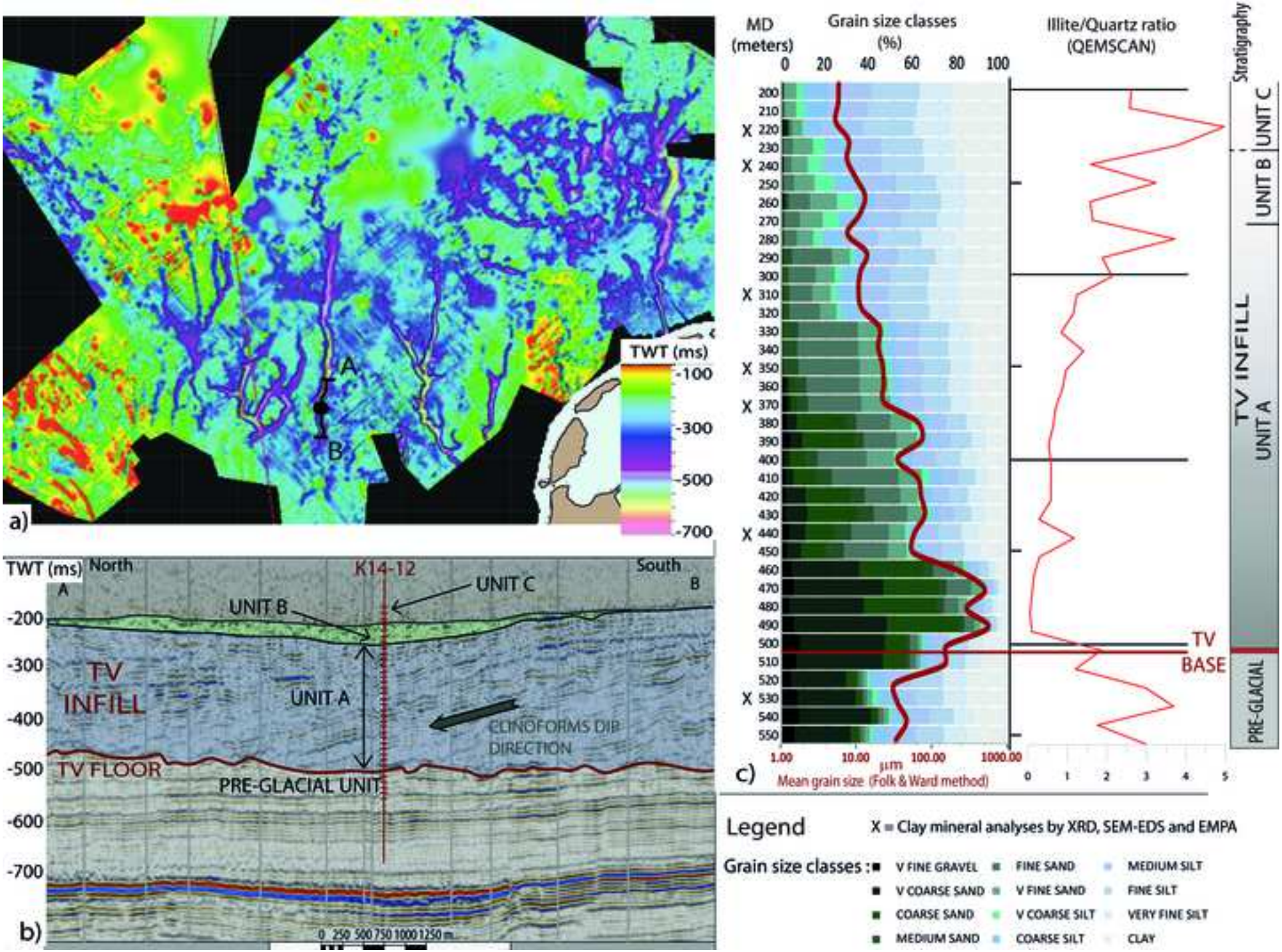

This is a 'pre-publication' version of an accepted article for Clays and Clay Minerals.
This version may be subject to change during the production process.
The DOI given, which may be used for citation purposes, though which will not be active until the version of record is published, is DOI: 10.1346/CCMN.2016.064026

Figure 3

Click here to download Figure Figure 3.tif

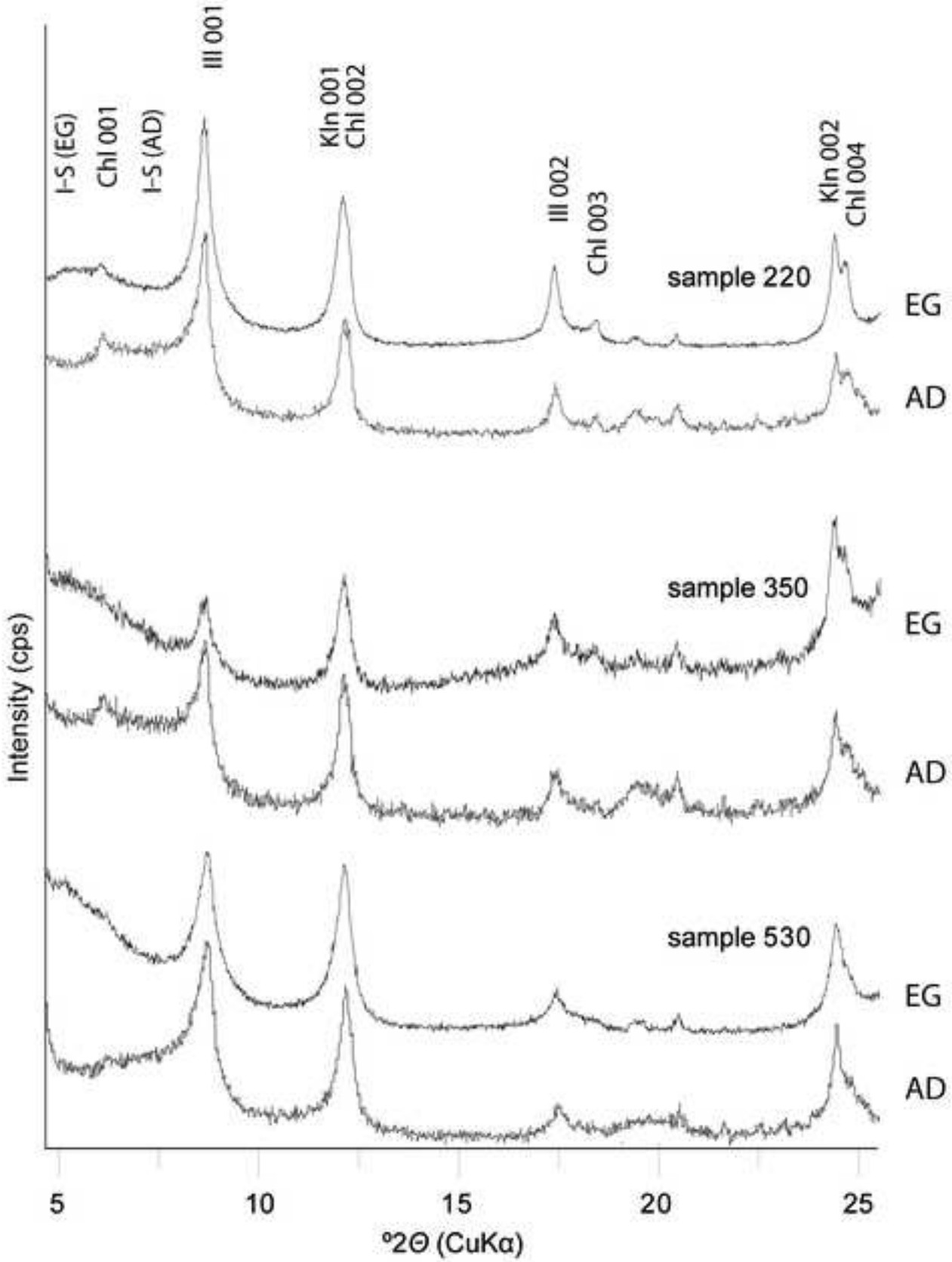

This is a 'pre-publication' version of an accepted article for Clays and Clay Minerals.
This version may be subject to change during the production process.
The DOI given, which may be used for citation purposes, though which will not be active until the version of record is published, is DOI: 10.1346/CCMN.2016.064026

Figure 4

Click here to download Figure Figure 4.tif

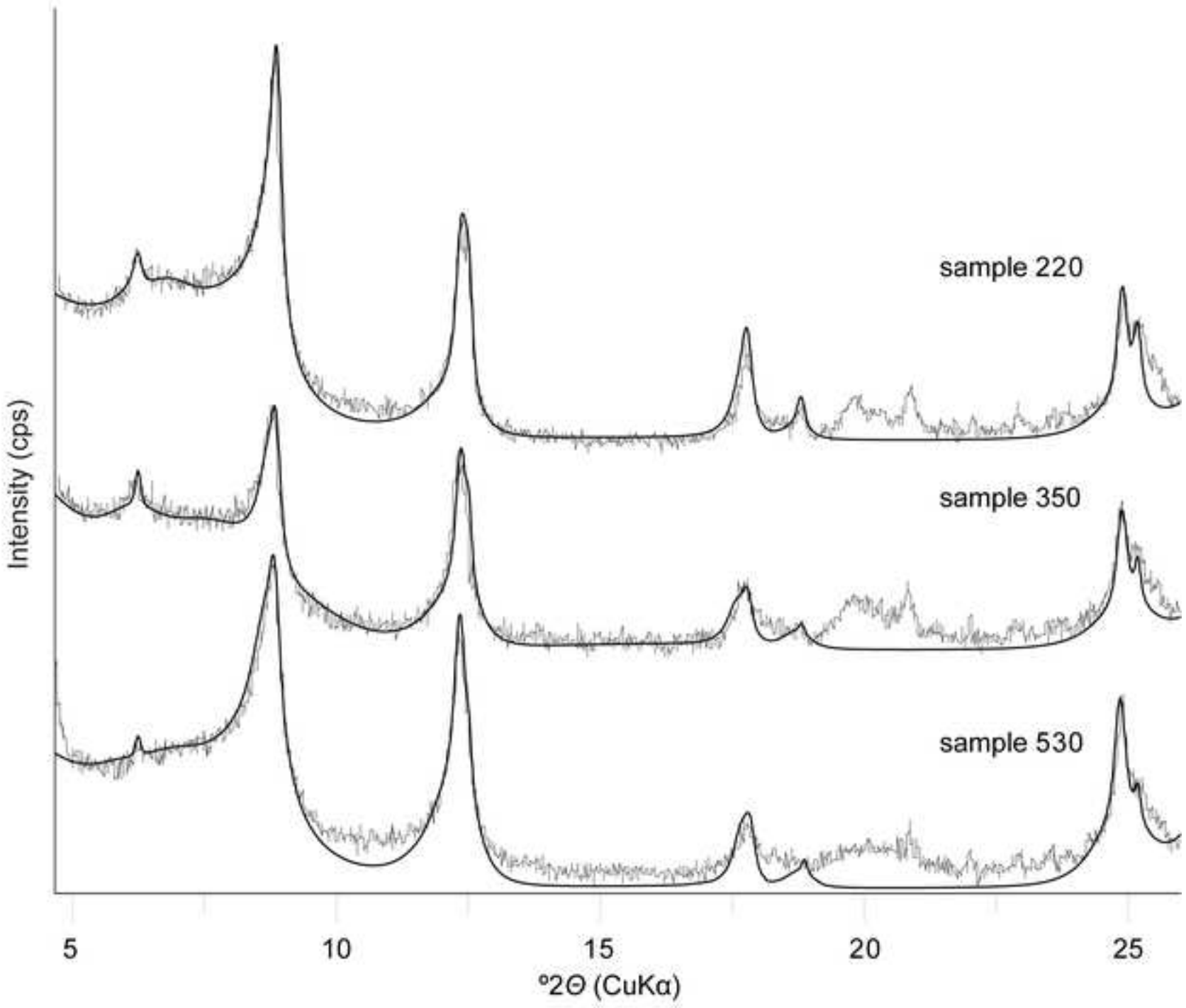

This is a 'pre-publication' version of an accepted article for Clays and Clay Minerals.
This version may be subject to change during the production process.
The DOI given, which may be used for citation purposes, though which will not be active until the version of record is published, is DOI: 10.1346/CCMN.2016.064026

Figure 5

Click here to download Figure Figure 5.tif

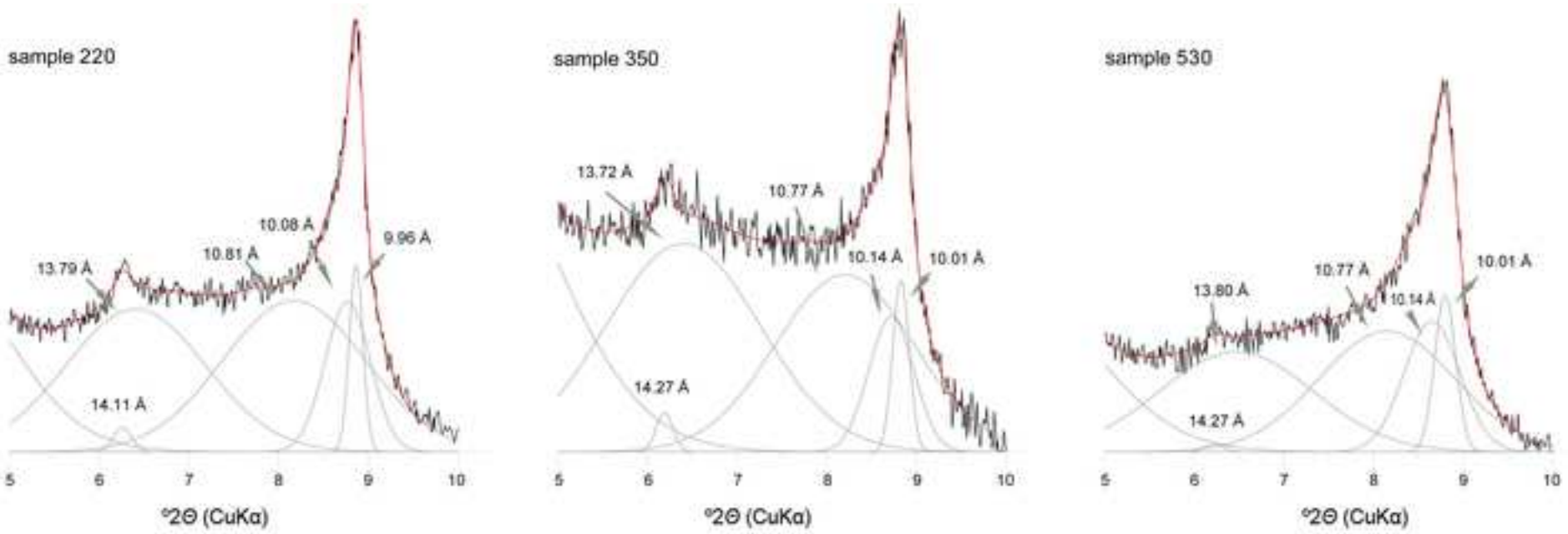

This is a 'pre-publication' version of an accepted article for Clays and Clay Minerals.
This version may be subject to change during the production process.
The DOI given, which may be used for citation purposes, though which will not be active until the version of record is published, is DOI: 10.1346/CCMN.2016.064026

Figure 6

Click here to download Figure Figure 6.tif

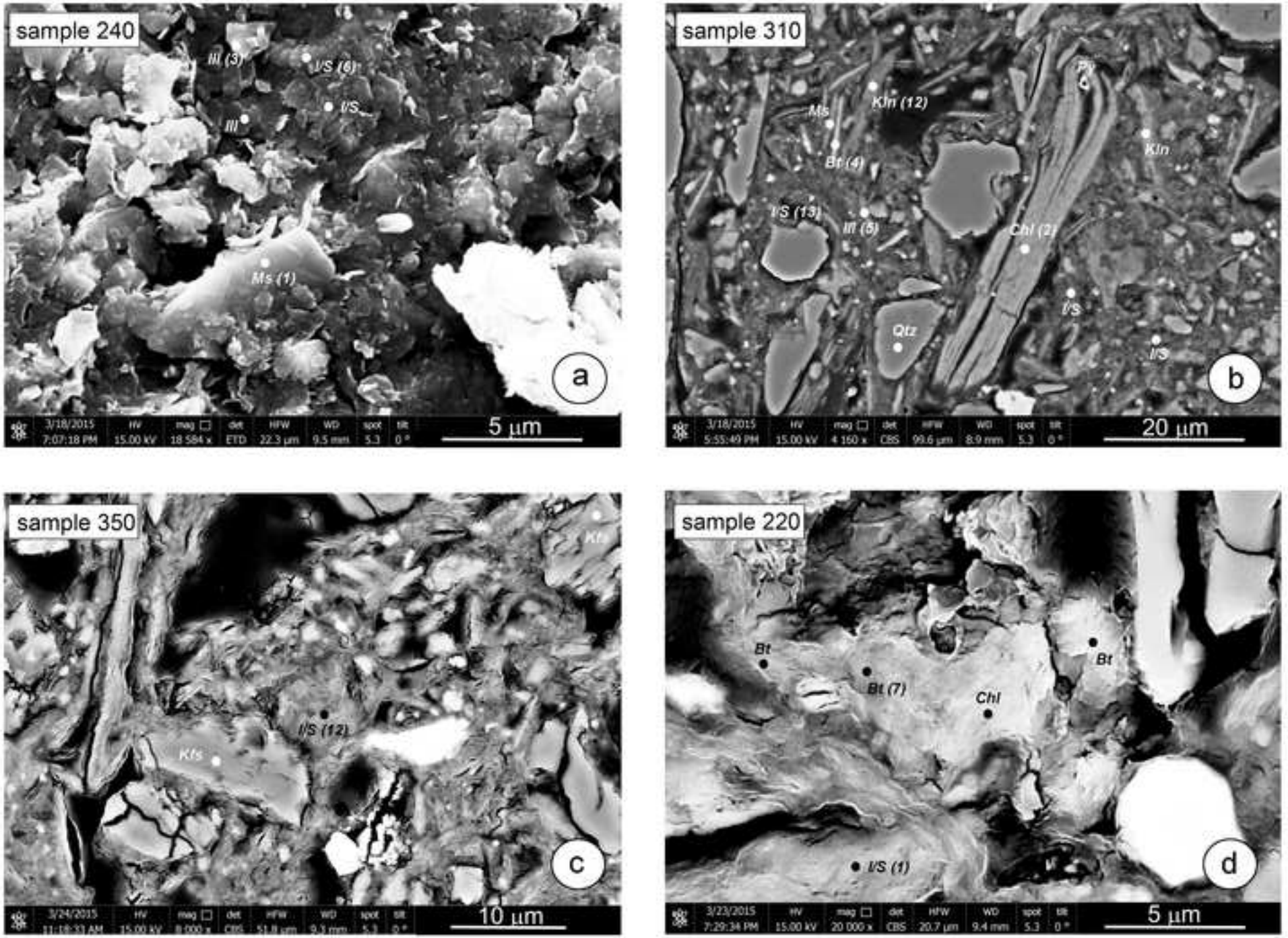

This is a 'pre-publication' version of an accepted article for Clays and Clay Minerals.
This version may be subject to change during the production process.
The DOI given, which may be used for citation purposes, though which will not be active until the version of record is published, is DOI: 10.1346/CCMN.2016.064026

Figure 7

Click here to download Figure Figure 7.tif

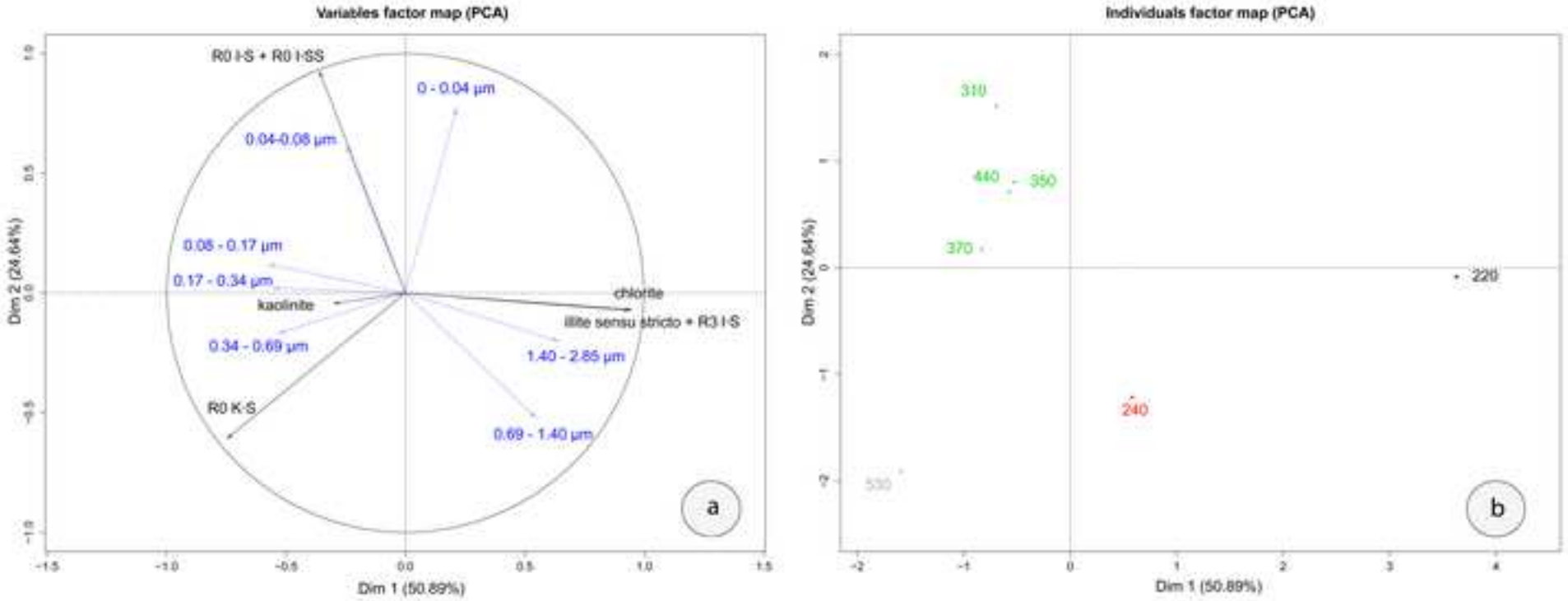

This is a 'pre-publication' version of an accepted article for Clays and Clay Minerals.
This version may be subject to change during the production process.
The DOI given, which may be used for citation purposes, though which will not be active until the version of record is published, is DOI: 10.1346/CCMN.2016.064026

Figure 8

Click here to download Figure Figure 8.tif

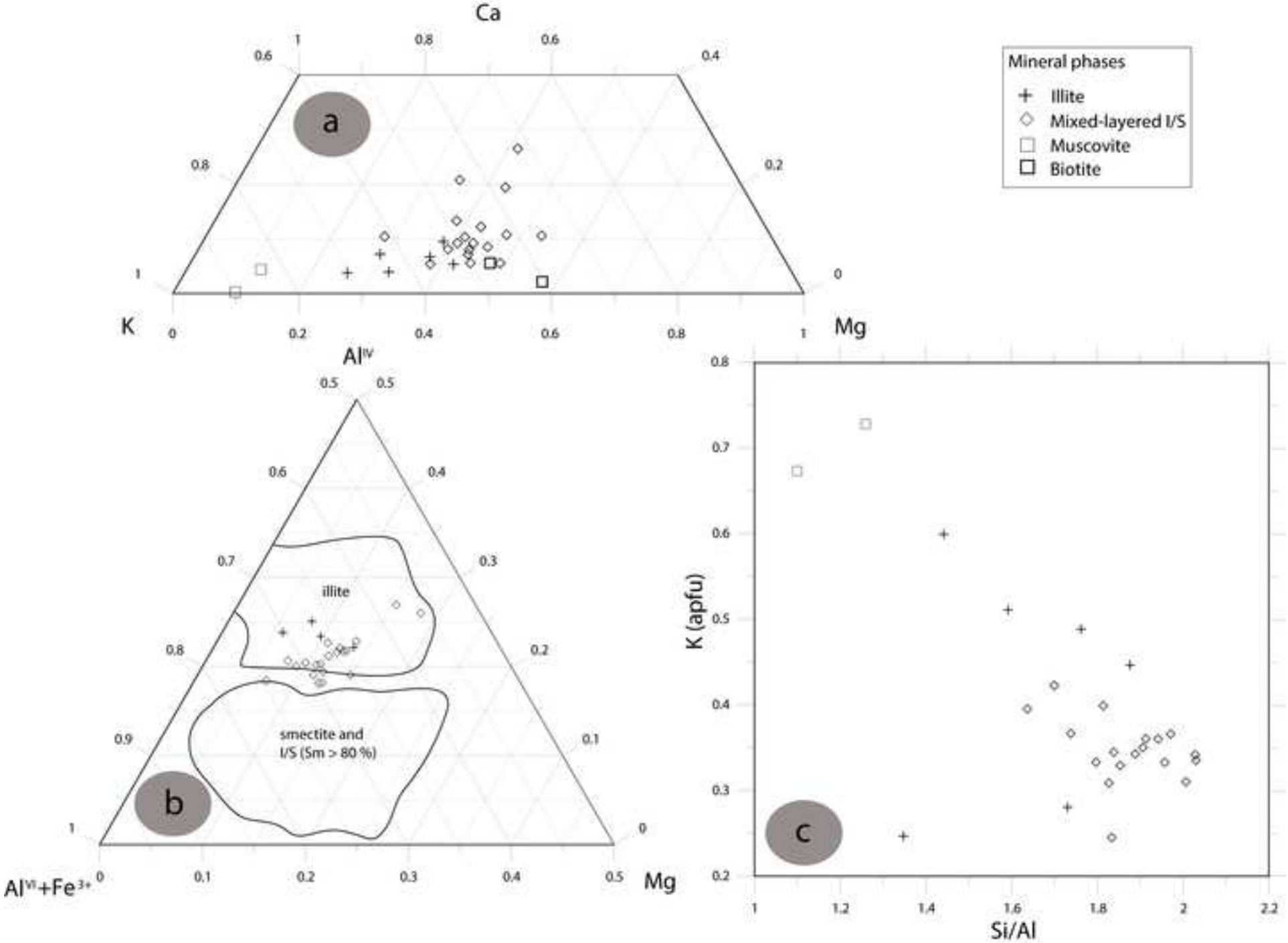

This is a 'pre-publication' version of an accepted article for Clays and Clay Minerals.
This version may be subject to change during the production process.
The DOI given, which may be used for citation purposes, though which will not be active until the version of record is published, is DOI: 10.1346/CCMN.2016.064026